DYNAMIC STRAIN AGING OF DUAL PHASE STEELS IN FORMING APPLICATIONS

A THESIS SUBMITTED TO
THE GRADUATE SCHOOL OF NATURAL AND APPLIED SCIENCES
OF
MIDDLE EAST TECHNICAL UNIVERSITY

BY

BERKAY BAYRAMİN

IN PARTIAL FULFILLMENT OF THE REQUIREMENTS
FOR
THE DEGREE OF MASTER OF SCIENCE
IN
METALLURGICAL AND MATERIALS ENGINEERING

SEPTEMBER 2017

Approval of the thesis:

DYNAMIC STRAIN AGING OF DUAL PHASE STEELS IN FORMING APPLICATIONS

submitted by **BERKAY BAYRAMİN** in partial fulfillment of the requirements for the degree of **Master of Science in Metallurgical and Materials Engineering Department, Middle East Technical University** by,

Prof. Dr. Gülbin Dural Ünver
Dean, Graduate School of **Natural and Applied Sciences** _____

Prof. Dr. C. Hakan Gür
Head of Department, **Metallurgical and Materials Engineering** _____

Assist. Prof. Dr. Mert Efe
Supervisor, **Metallurgical and Materials Eng. Dept., METU** _____

Assist. Prof. Dr. Caner Şimşir
Co-Supervisor, **Manufacturing Eng. Dept., Atılım University** _____

Examining Committee Members:

Prof. Dr. Cevdet Kaynak
Metallurgical and Materials Eng. Dept., METU _____

Assist. Prof. Dr. Mert Efe
Metallurgical and Materials Eng. Dept., METU _____

Prof. Dr. Arcan Dericioğlu
Metallurgical and Materials Eng. Dept., METU _____

Assist. Prof. Dr. Sezer Özerinç
Mechanical Eng. Dept., METU _____

Assist. Prof. Dr. Kemal Davut
Metallurgical and Materials Eng. Dept., Atılım University _____

Date: 06.09.2017

I hereby declare that all information in this document has been obtained and presented in accordance with academic rules and ethical conduct. I also declare that, as required by these rules and conduct, I have fully cited and referenced all material and results that are not original to this work.

Name, Last name : Berkay Bayramin

Signature :

ABSTRACT

DYNAMIC STRAIN AGING OF DUAL PHASE STEELS IN FORMING APPLICATIONS

Bayramin, Berkay

M.S., Department of Metallurgical and Materials Engineering

Supervisor: Assist. Prof. Dr. Mert Efe

September 2017, 69 pages

Sheet metals are subjected to certain temperatures (25-200^{o}C) and strain rates (1-10 s^{-1}) during forming applications. These thermomechanical conditions may cause dynamic strain aging (DSA) in various grades of steels including dual phase (DP) steels. DSA represent itself as serrations in the stress-strain curves. Two grades of DP steels (DP590 and DP800) were studied systematically at different strain rates ($10^{-3}s^{-1}$-$1s^{-1}$) and temperatures (25^{o}C-400^{o}C) to investigate the DSA effects on the mechanical properties and formability. Test results show that DSA controls the deformation behavior between 200^{o}C - 300°C through serrations in the stress-strain curves of both grades. Increasing strain rates between these temperatures result in severe drops of uniform and total strain. Also with increasing negative strain rate sensitivity (NSRS) these drops in the ductility state weak formability. Besides the tests to identify DSA, a simple microstructural model on dislocation motion is developed to explain the responsible mechanisms for DSA and its effects on the jerky-serrative flow behavior.

Keywords: Dual-Phase Steels, DSA, Formability, Warm Forming, Dislocation Cells

ÖZ

İKİ FAZLI ÇELİKLERİN ŞEKİLLENDİRME UYGULAMALARINDA DİNAMİK GERİNİM YAŞLANMASI

Bayramin, Berkay

Yüksek Lisans, Metalurji ve Malzeme Mühendisliği Bölümü

Tez Yöneticisi: Yard. Doç. Dr. Mert Efe

Eylül 2017, 69 sayfa

Metal levhalar endüstriyel şekillendirme prosesleri sırasında belli başlı sıcaklık (25-200^{o}C) ve gerinim hızlarına (1-10s^{-1}) maruz kalmaktadır. Bu termomekanik koşullar iki fazlı çeliklerin de içinde bulunduğu çok sayıda çelikler üzerinde dinamik gerinim yaşlanmasına (DGY) yol açabilir. DGY gerilim-gerinim eğrileri üzerinde kendini tırtıklı-dalgalı bir yapıda belli eder. Bu çalışmada, DGY'nin mekanik özellikler ve şekillendirilebilirlik üzerindeki etkilerinin sistematik bir şekilde araştırılması amacı ile iki farklı DP çeliği (DP590 ve DP800) farklı gerinim hızları ($10^{-3}s^{-1}$-$1s^{-1}$) ve sıcaklıklar (25^{o}C-400^{o}C) altında test edilmiştir. Test sonuçları 200^{o}C-300°C arasında DGY etkinliğini, iki çeliğin gerilim-gerinim eğrileri üzerindeki tırtıklı-dalgalı davranışlar sonucu ortaya koymuştur. Bu sıcaklıklar altında artan gerinim hızları sonucu tek düze ve toplam gerinimdeki düşüşle beraber ortaya çıkan diğer bir etken olan ters gerinim duyarlılığı, süneklikte bir düşüşe neden olup malzemenin

şekillendirilebilirliğinde bir zayıflığı ima etmektedir. DGY'nin mekanik özellikler üzerindeki etkilerini incelemek üzerine yapılan testlere ek olarak, dislokasyon hareketine dayalı bir mikroyapısal model DGY'den sorumlu mekanizmalar ve tırtıklı-dalgalı eğrilerin açıklanması için geliştirilmiştir.

Anahtar Kelimeler: İki Fazlı Çelikler, Dinamik Gerinim Yaşlanması, Şekillendirilebilirlik, Ilık Şekillendirme, Dislokasyon Hücreleri

To my beloved family...

ACKNOWLEDGEMENTS

This work was supported by TÜBİTAK project #115M642. The testing materials were supplied in collaboration with Sinan Küçük from SSAB-Turkey with his great effort in bureaucratic work. Additionally, a journal article is utilized in this thesis.

I feel so indebted to my advisor Assist. Prof. Dr. Mert Efe for his nonstop support, faith on myself, encouragement, kindness, and approach on the problems that I encountered during this study. He had never stinted his academic knowledge and experience from me during my whole study. It would be impossible to complete without his guidance. I am also grateful to my co-advisor Assist. Prof. Dr. Caner Şimşir for his great effort together with his guidance and knowledge that he delivered to me all the time. I felt myself very confident knowing his support behind me.

I am also in a deep appreciation to Dr. Süha Tirkeş who gave all that he got whenever I needed help. Special thanks to my friend Umutcan Ertürk in all my academic and social life during this period is my debt of gratitude. My lab mate Baran Güler who is a man of discipline and efficiency, backed me up every time. Also my lab mates Kıvanç Alkan and Yılmaz H. Akın gave their mental and physical support all time. Special thanks to my friends Ethem Bozkurt, Uygar Çelik, Eren Pinaz, Kadir Akar, Batuhan Aydoğan, Yusuf Karslı, Engin Dizlek, Ahmet Oğuz Yaman, Barış Evran, Eren Çelik, Servet Arpacı and Yetkin Şibil is a must.

She is the one who entered my life and took my heart, Elif Özlem Güner. I love you forever.

Last but not least, I owe to my father İlhami Bayramin and my mother Suay Bayramin. They have never lost their faith and support on me.

TABLE OF CONTENTS

LIST OF TABLES

TABLES

LIST OF FIGURES

FIGURES

CHAPTER 1

INTRODUCTION

In the last decades, the demand for energy saving, efficiency, economic fuel consumption, value, repair ability and lightweight production become an open-ended challenge, especially in the automotive industry. In conjunction with lightweight fabricating, passenger safety and the performance of the vehicle must be in acceptable and efficient limits. With a greater combination of strength and ductility compared to the conventional high strength steels (HSS), advanced high strength steels (AHSS) are introduced to fulfill these requirements. AHSS is currently in a large percentage of weight usage in most of the new generation automobile body structures. AHSS usage in automobile frame and structure is currently the most suitable choice. Some of the common brand new generation automobile structures are illustrated in Figure 1 [1–4]. The dominance of the weight percentage of AHSS established on the vehicles bulk body structure can be clearly seen in Figure 1 for some heading brands. This dominance proves the increasing trend on AHSS steels, also mentioned in Figure 2 [5] which is estimated to reach nearly double of its percentage from today, in future years.

The key reason of AHSS access in automobile structure is due to steels strong ability to endure in major considerations, such as crash and high strength [6], thus allowing thinner thickness and gauge to be established in the structure [7]. Figure 3 [8] shows the range of mechanical properties available from conventional steels to today's AHSS steels. Some grades of AHSS can hold up to 4 times of strength compared to conventional grades besides retaining high ductility. High strength combined with great toughness relies on the multi-phase structure.

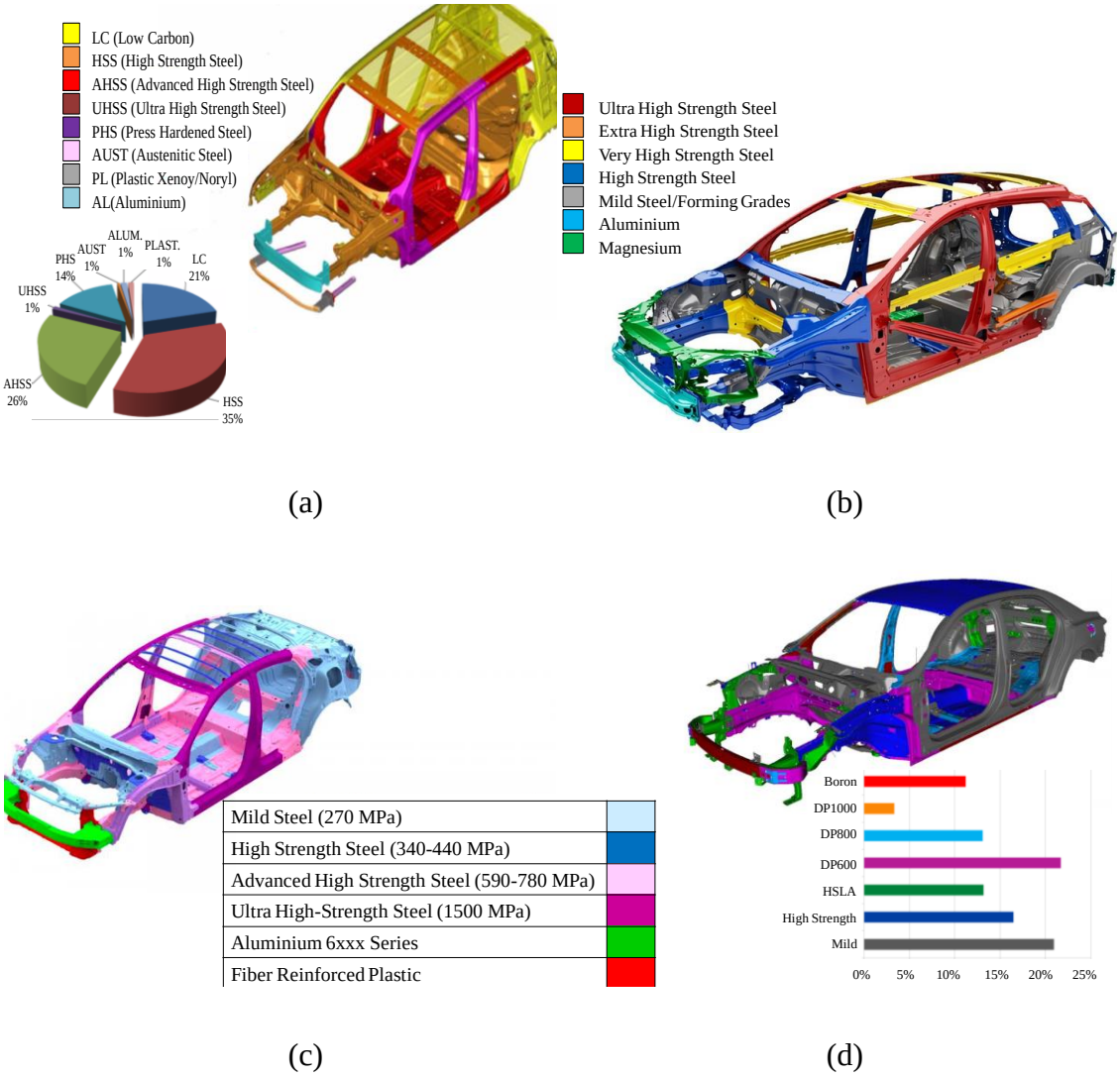

Figure 1 Schematic view of body structures of some new generation automobiles (a) 2017 Jeep Renegade [1], (b) 2010 Volvo S60 [2], (c) 2016 Honda Civic [3], (d) 2016 Lincoln Continental [4]

Unlike lightweight alloys like aluminum and magnesium, AHSS covers the safety standards of National Highway Traffic Safety Administration (NHTSA) agency [9] and Corporate Average Fuel Economy (CAFE) [10] entirely. Besides stiff crash performance and high strength, these steels are also cost efficient. AHSS generates these improved mechanical properties cheaper through precise thermo-mechanical processing rather than grades like high strength low alloys (HSLA) which are processed by alloying and solid solution hardening.

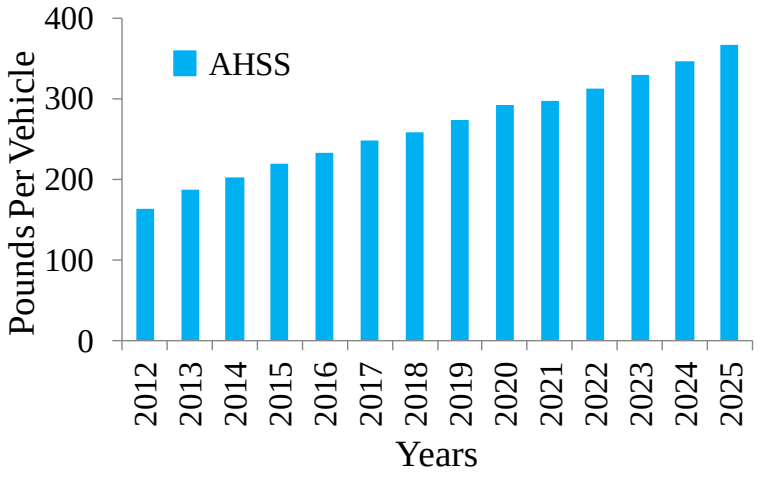

Figure 2 North American light vehicle AHSS utilization forecast (source: Ducker Analysis) [5]

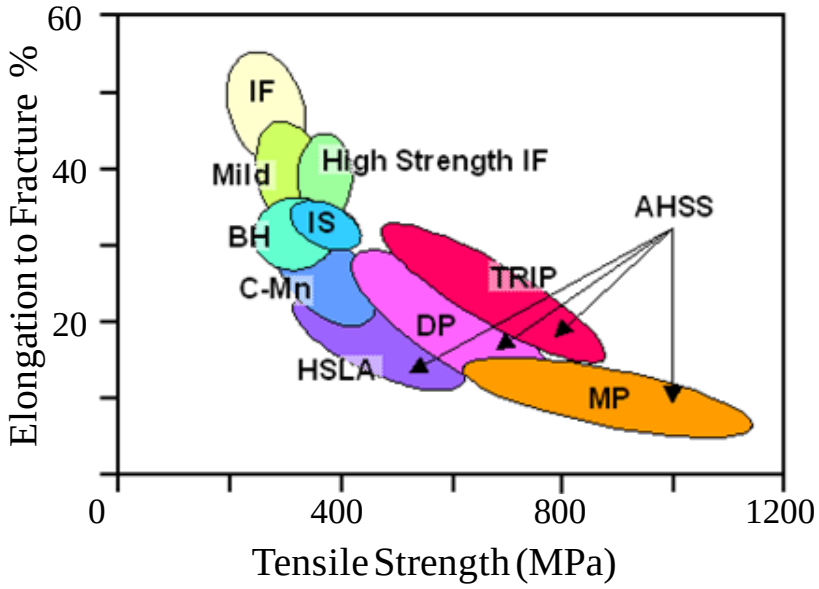

Figure 3 Ductility vs. strength diversity of high strength steel grades available today [8]

Some other advantages of AHSS steels are good weldability (also possible with all conventional methods), life cycle (repeatable use), low greenhouse gas (GHG) emission, stiffness (stable riding and steering), durability (long fatigue life under dynamic conditions) and good formability [10].

AHSS family consists vast types of steels, mostly multi-phased microstructure, like dual-phase (DP), transformation induced plasticity (TRIP), complex phase (CP), hot-formed (HF), twinning induced plasticity (TWIP), ferritic-bainitic (FB) steels. Each type of these steels supplies unique applications to meet the best combination of the mentioned requirements. DP steels are most likely preferred as the structural material at the core parts of the automobile, which are chassis and body structure. Lean alloying of a low carbon steel and passing through basic thermomechanical processes is a big advantage to provide high strength and ductility by staying in the limit of environmental and economical charges [11]. The elegant combination of high strength and high ductility of DP steels ensures good crash performance together with all other aforementioned efficient features that AHSS provide. Besides the vastly reported microstructural studies in the literature [12–16], deformation parameters such as strain rate and temperature may have significant effects on the mechanical behavior of DP steels on strength and ductility [17–19]. Since crash means high strain rate, DP steels at high strain rates are vastly studied [18,20–22].

Parameters of deformation processes also become important while manufacturing complex shaped parts of applications in sheet forming. Automotive sheet forming vary in a wide range of temperature (-40-100^{o}C) and strain rates (10^{-4}-10^{3}s^{-1}) [23]. Moreover, the local temperature rise in forming of DP sheets at room temperature is also reported [24]. Therefore, the automotive industry is in need of data which illustrate mechanical and forming limits of DP steels, especially at intermediate strain rates like 1-10s^{-1}. At elevated temperatures and high strain rates, loss of ductility and significant strengthening could be a threat to the forming process [19]. This effect shows its' symptoms mostly as consecutive serrations in the stress-strain curves, which is linked to dynamic strain aging (DSA) in DP steels [25,26].

As being one of the most common symptoms of the DSA, serrations may lead the material towards an unstable mechanical response in the form of ductility loss with increasing temperature and deteriorate the formability of the parts. Yet, there is no extensive work done covering the forming parameters strain rate (1-10s^{-1}) and temperature (RT-300^{o}C) of DP steels, relevant to industrial forming applications. Thus, a systematic work is in need for the forming limits of DP steels which correspond to intermediate strain rates and temperatures whereas DSA may dictate the whole forming processes.

In this study, we investigate the mechanical behavior of two different grades of DP steels, DP590 and DP800, with well-controlled constant strain rate and temperature experiments between strain rates $10^{-3}s^{-1}$-$1s^{-1}$ and temperatures 25^{o}C-400^{o}C. Within these conditions, we identify the critical temperatures and strain rates for the DSA and compare the two DP grades to investigate the effects of microstructure on the DSA behavior. Parallel to the mechanical test results, we explain the DSA mechanisms in these steels by X-ray measurements of dislocation density and a model based on the dislocation motion in the ferrite phase.

CHAPTER 2

LITERATURE REVIEW

2.1 DP Steels

Being formed of a mixture of martensite and ferrite, DP steels present a wide range of toughness and strength [6]. The softer phase ferrite provides toughness and elongation while the harder phase martensite establishes the strength.

The chemistry of DP steels typically match with plain carbon steels just with a slightly more amount of manganese and may have an addition of niobium, molybdenum and chromium, vanadium to increase the hardenability [10]. However, the element significantly affecting the hardness of the steel is carbon [27]. The higher carbon content means higher hardening which can be seen as an increased martensite fraction (carbon pinning in the lattice), resulting in an increase in the strength. Some other properties of DP steels are generalized in Table 1.

Table 1 General features of a DP steel [10]

Properties of DP Steel	
Microstructural Features	Soft ferrite matrix, hard martensite islands
Formability	Excellent
Weldability	Good, requires good schedule at high strengths
Typical Additions	C,Si,P must be balanced for weldability, Mn,Cr,Mo,V for hardenability
Performance	Resists fracture, delays necking, good manufacturing
Applications	Beams, cross members,structural components, crash energy absorption

2.2 Processing of DP Steels

Various methods are obtained to shape the steel into the desired and intended conditions for use. Strengthening mechanisms in use are typically solid solution strengthening, grain refinement, work hardening, precipitation hardening and transformation hardening as well. As it is evident from its name, DP steels are generally produced by transformation hardening from the intercritical region (γ+ α) which consists the steps of annealing and quenching, respectively.

2.2.1 Obtaining DP Steels by Controlled Cooling from the Intercritical Region

For most of the AHSS, including DP steels, controlled cooling from the intercritical γ+α region is the main manufacturing process [15]. Between the T_2 and T_1 temperatures, controlled parameters such as heating rate, annealing temperature, cooling character and tempering conditions allow obtaining the combination of the desired microstructure during the process [28]. To establish chemical homogeneity together with isothermal austenite growth, being attentive on the intercritical holding time is a significant point [28].

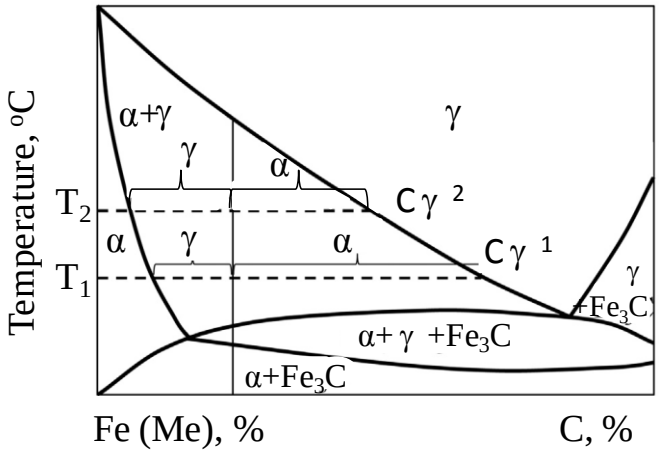

Figure 4 Pseudo-binary phase diagram of Fe(Me)-C, (Me) implies a second alloying element [28]

The pseudo-binary phase diagram of Fe(Me)-C in Figure 4 estimates the amount of austenite maintained at the end of the holding time in the range of annealing temperatures with respect to the carbon level of the steel. Following the colored linear line by cooling is shown as an example of defining the phase ratios with respect to the lever rule. As distinguished from the ineligible time for equilibrium, the activity of initial microstructure, heating time, distribution of the alloying elements can shift the intended ratio of the phases [28].

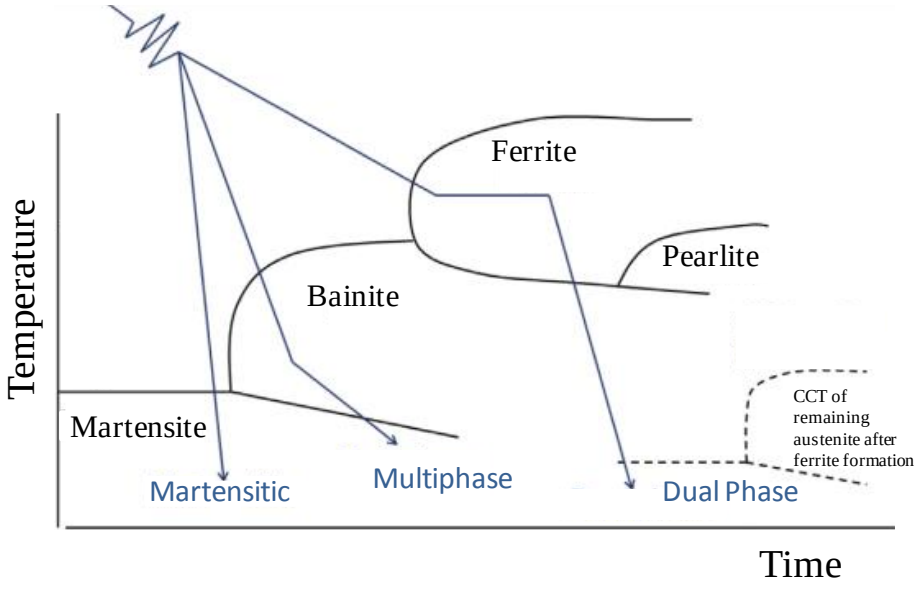

Figure 5 Scheme of the phase production [29]

As it is illustrated in Figure 5, cooling time is the main parameter that constitutes the phase type. Fast cooling following annealing at the intercritical region transforms austenite into martensite. Longer time spent on cooling stabilizes bainite, ferrite, and pearlite, respectively. These mechanisms are generally controlled in thermomechanical manufacturing processes, where the rolling process takes place in the austenitic zone.

2.3 Mechanical Properties of DP Steels

2.3.1 Strength

The volume fraction of the phases primarily states the mechanical strength. Many number of studies mark that martensite fraction controls the tensile strength [30–32]. Due to its rigid and stiff structure, the martensite phase can carry a serious amount of load transferred from the ferrite. Figure 6 [30] illustrates the increase in tensile strength with increasing martensite fraction for DP steels with respect to 3 different carbon fractions. It is clear from the figure that increase of the carbon content at constant volume fraction of martensite is also a factor that increases the tensile strength. Note that the steels were intercritically annealed followed by water quenching in Figure 6.

On the other hand, martensite morphology plays an important role on the strength. In a reported study [33], fibrous martensite structure containing DP steel shows higher strength compared to the network martensite structured DP steel. The reason for this behavior is reported as the better distribution of the fibrous martensite structure is stronger than the network martensite morphology.

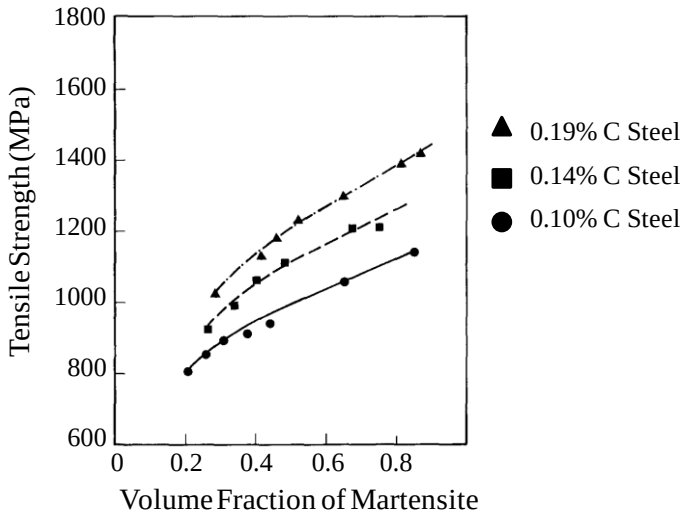

Figure 6 Tensile strength versus martensite fraction of a DP steel in different C contents [30]

When the amount, size, morphology or the distribution of the individual phases are changed, the strain incompatibility between the two phases differentiates distinctly [20]. A dual-phase structure with a serious amount of high martensite shows increased strength corresponded by a decrease in ductility. Phase distribution could also control the mechanical properties and cause unstable responses of the material through deformation, if non-homogeneity exists. A localization of an individual phase could shift the mechanical properties towards its nature (martensite on higher brittle behavior, ferrite on higher ductility and elongation). The morphology of the martensite, as mentioned before, is a significant effect that influences the mechanical properties. Thus, this result of being under the influence of a strain mismatch between the phases ends up with a shift of the mechanical behavior of the material towards the dominant phases responds against loaded stresses. As a result, these properties should be detected with attention during forming application to meet the desired results.

2.3.2 Ductility

DP steels show higher elongation compared to some other AHSS like high strength low alloy (HSLA) and multiphase (MP) steels (Figure 3). However, as the amount of martensite increases uniform and total elongation shows a clear decrease which is a negative fact for the use of sheet forming. A systematical work has been reported [34] on DP steels, implying this effect of martensite by a group of tests under intercritical annealing temperatures 740^{o}C, 760^{o}C, 780^{o}C which is illustrated in Figure 7. Also the intercritical temperature increase is reported to increase the ductility of the steel.

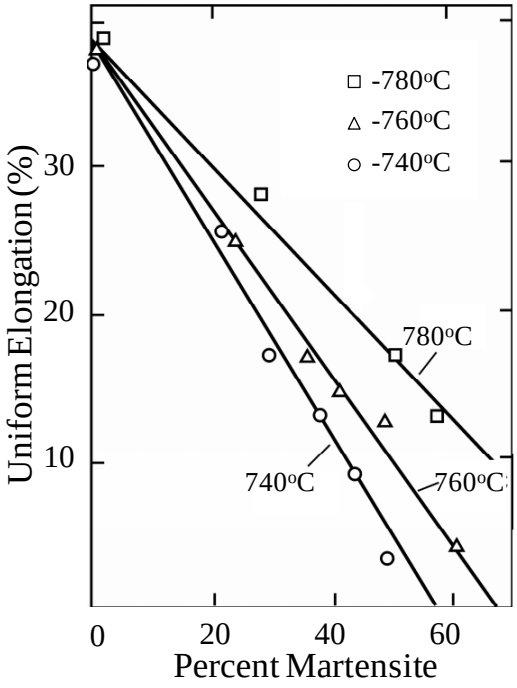

Figure 7 Uniform elongation (%) with respect to martensite [34]

The addition of elements in steel composition is proved to be resulting in an increase of ductility of DP steels. Since ferrite controls the ductility of a DP steel, stabilizing ferrite would maintain the steel to be more ductile. Ferrite strength could also be adjusted with substitutional solute additions like Mn, P and Si ferrite strength is managed to be shifted higher [35]. The addition of Si is the most effective in increasing ductility of ferrite between the mentioned three. Higher strain hardening has an outcome of higher uniform elongation and an improved balance of tensile strength-ductility at high Si levels [29]. However, the addition of P decreases ductility faster than it increases the strength of the steel [35]. Al addition was also reported resulting in an increased balance of strength-ductility due to the better formation of the refined ferrite structure and smaller sizes of discontinuous martensite islands [36].

2.3.3 Forming Behavior of DP Steels

DP steels are used in critical parts of products in industries like aerospace and automotive. These critical parts are mostly the complex formed body and chasis structures. Unlike the conventional steels, DP steels can show deterioration under forming conditions more frequently due to the complex microstructure it consists. Local temperature raise contributed with high strain rates could lead failure ending up with diminution. Due to the challenge to form these kind of important structural parts the forming processes require a precise attention.

Forming processes of DP steels, especially in the automotive industry, is generally held in the cold forming region ($T < 0.35T_{melt}$) by taking advantage of strain hardening under high forces applied. Due to the complex microstructure of DP steels, hot forming ($T > 0.55T_{melt}$) is not an option to choose, or else the good mechanical properties that the material provides may dissipate at high energy levels. Moreover, much better hot formable materials could be chosen instead of DP steels. Warm forming ($0.35T_{melt} < T < 0.55T_{melt}$) , is an intermediate forming region to avoid high temperatures and forces which could allow recovery but not recrystallization [37]. Despite the forming of DP steels are mostly processed under cold working temperatures, sometimes warm forming temperature region could be reached locally due to the deformation heating in complex shaped regions during the forming of the material. Therefore, it can be assumed that forming of DP steels experience both cold and warm forming temperatures.

Forming of sheet metals could be characterized in two scales. Besides macro features and forming techniques, formability also strongly depends on microstructural facts. Both of these facts are taken in detail in the further sub-sections.

2.3.3.1 Macro-Mechanical Forming

Forming of sheet steels deeply require stretch formability, high bending ability, high deep drawing ability.

In forming processes, control of these forming parameters has a great importance which is strongly bonded to the microstructure and the texture of the material [38]. As mentioned before, DP steels can be produced in various hot-rolled thicknesses in the intercritical zone either by the hot-strip milling process or a post-roll annealing [39]. Butler and Bucher's [40] report on DP steels visualizes the high strength-ductility compared to some other grades, which is illustrated in Figure 8. Their strength-ductility data laps on a different curve than ferrite-pearlite and plain carbon steels. This result means better formability of DP steels rather than ferritic-pearlitic and plain carbon steels. They workharden very rapidly at low strains [35] and they reach their ultimate tensile strength (UTS) at higher strains compared to their yield strength. Therefore DP steels exhibit a high gap between the UTS and the yield point which points out a low yield strength (YS)/UTS ratio. This low ratio means much more uniform elongation, and hence, much more formability of DP steels.

High impact energy absorption is another criterion of good formability considering sheet metal forming. The magnitude of the impact energy absorption could be used to define sheet metal formability. The relationship between the quasi-static flow stress (%5) and value of absorbed energy is highlighted in Figure 9 [41].

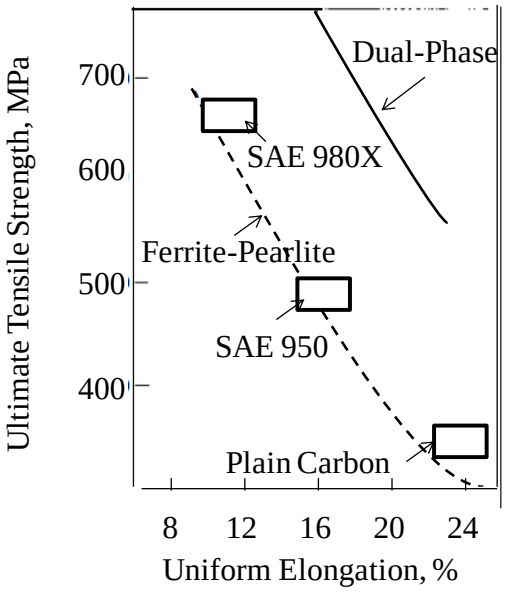

Figure 8 Strength-ductility comparison of different grades of steels [40]

The DP and TRIP type steels absorb a distinctly high magnitude of energy which also corresponds to a high magnitude of stress compared to the other grades solution hardened, bainitic and precipitation hardened steels. This is another fact that highlights the good formability of DP grade steels.

Through all of these facts, most reliable indicators of the formability concern are the strain hardening exponent, strain rate sensitivity and temperature, denoted as "n", "m" and "T", respectively. The attainment of the material to pass the strain across parts is defined with higher values of the strain hardening exponent. Table 2 represents the typical mechanical properties of three different grades of DP steels. The higher strain hardening exponent value corresponds to higher elongation, which also means much more ductility and strain hardening.

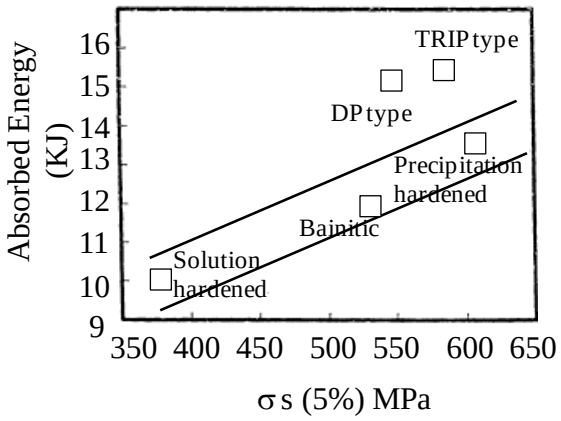

Figure 9 Representation of formability with respect to quasi-static flow stress and impact energy [41].

Therefore, forming applications of high value of strain hardening exponent consisting steels may be estimated as much easier to form into the final product. DP590 steel listed in Table 2 has a high value of strain hardening exponent, which is more formable than the other grades of DP steels listed.

Despite the low values of the strain hardening exponent of the other grades of steel have, the low YS/UTS ratio still exists which implies good formability of DP steels.

Beside the strain hardening exponent, strain rate sensitivity is another major factor that controls the limits of the forming processes. Loading a material with different strain rates could result in different stress-strain curves. This means that the material is strain rate dependent. Strain rate sensitivity is defined as the factor that prevents the possibility of strain concentration in a local area. Higher value of strain rate sensitivity implies higher formability for sheet metals.

Both strain hardening exponent and strain rate sensitivity controls the materials forming prosess. However, in some forming conditions of DP steels these two factors could decrease and cause the forming processes to be more challenging to finalize the desired product. Therefore, it is critical to pay attention on these forming parameters.

Table 2 Typical properties of 3 different grades of DP steels [42]

Grade	Yield Strength MPa	Tensile Strength MPa	Elongation in 50 mm (%)	n-value calculated between 4% and 6% strain	n-value calculated between 10% strain and uniform elongation
CR330Y590T-DP	330-430	590-700	⩾21	⩾0.18	⩾0.14
CR440Y780T-DP	440-550	780-900	⩾15	⩾0.15	⩾0.11
CR590Y980T-DP	590-740	980-1130	⩾11	n/a	n/a

In light of all the macro-mechanical components mentioned, in consideration of metal forming, forming limit diagrams (FLD) were introduced in the 1960s and therefore to prevent forming failures to state the localized thinning which starts to initiate the failure. The forming limit curve is introduced as a plot of major and corresponding minor principal strain. Experimentally collected major and minor principal strain data constitutes these diagrams where the values of failure and necking strain give the failure zone of forming. The FLD must be determined through precise and detailed experimental analyses. An example of a forming limit curve is given in Figure 10. Colored zones in the figure point out the zones to stay in or the to be avoided in applications of sheet forming. Therefore it can be easily handled during industrial forming processes to form the sheet metal into the desired final product.

The FLD's were just introduced on the purpose of a brief on metal forming. The forming perspective of this study does not cover the development of FLD's of DP steels, however the conditions that increase and decrease the formability of DP steels are identified.

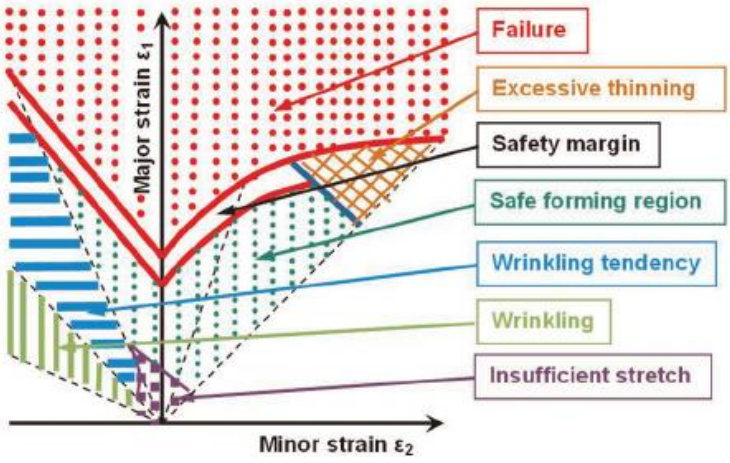

Figure 10 Schematic representation of a forming limit diagram with regions [43]

2.3.3.2 Microstructural Aspects of Forming

Non-homogeneity and the complex morphology of the phase distributions have been a title of interest for many researchers. The general deformation process is thought to be initiated in the ferrite phase [44]. Korzekwa et al., [45] found an initial dislocation density gradient near the martensite islands, meanwhile ferrite stays in with a lower magnitude of dislocation density. Under deformation, this gradient starts to spread inside the ferrite grains.

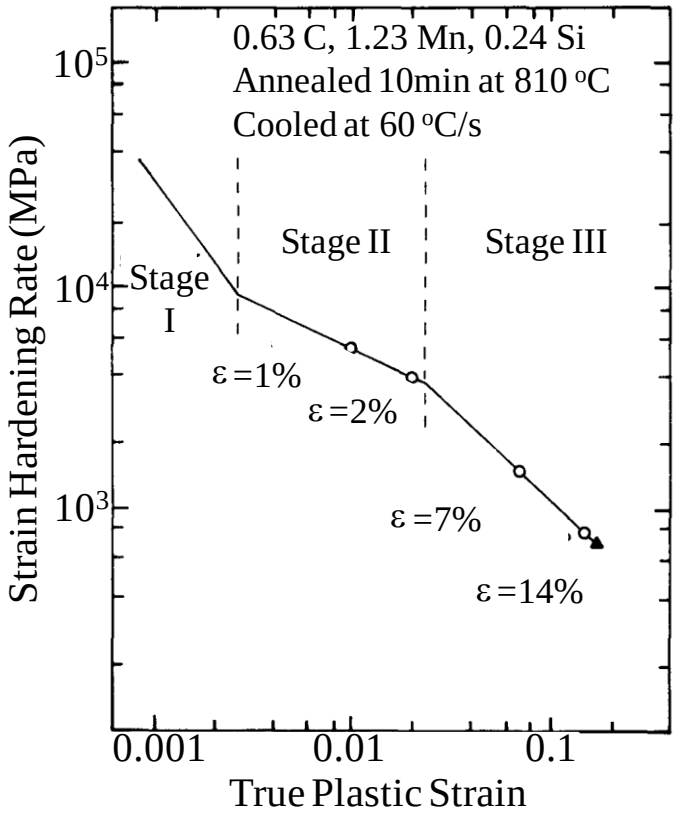

Figure 11 Jaoul-Crussard plot of a DP Steel [45]

As the strain increases, the dislocations start to build a dislocation cell network. According to the data collected and adapted by Korzekwa et al., [45] into the Jaoul-Crussard analysis in Figure 11, a three stage strain hardening is illustrated with respect to strain hardening rate and strain.

Stage I starts with a large number of dislocations concentrated near the martensite islands (no strain). These dislocations are defined as geometrically necessary dislocations (GNDs), as they are created to resume the contact between the two phases [46].

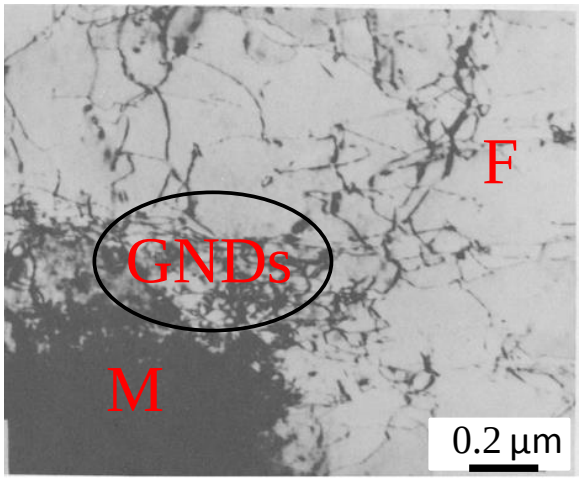

(a)

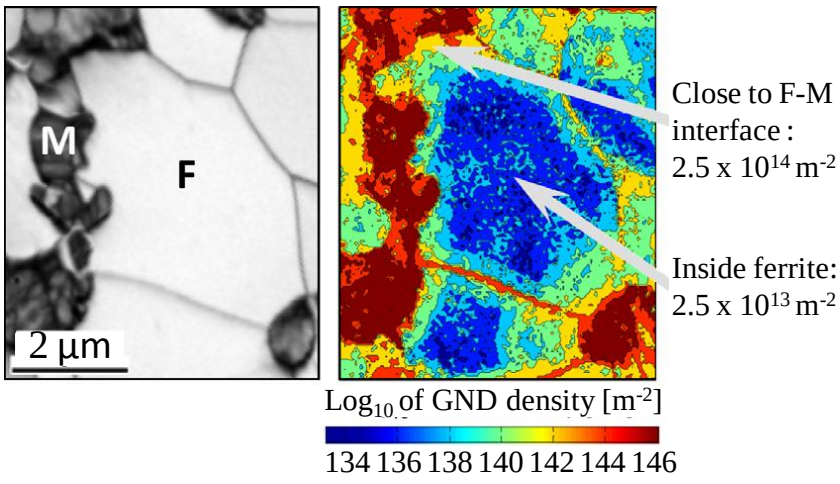

(b)

Figure 12 (a) Dislocation substructures observed in a DP steel. F-ferrite, M-martensite, GNDs-Geometrically necessary dislocations [45] (b) KAM method GND measurement in the microstructure [47]

Figure 12 (a) represents ferrite, martensite-ferrite and martensite zones of an as-received DP steel [45].

High concentrated dislocation density near the ferrite-martensite border is in sight. Dislocation density decrease in the ferrite grain interior. This difference of initial dislocation densities in a dual-phase microstructure is also sighted in later work reported by Kadkhodapour et al., [47] according to the kernal average misorientation method (KAM, Figure 12 (b)) which is sighted to be very appropriate for the calculation of the GND densities by Calcagnotto et al., [48]. Stage I (<0.1%), in Figure 11 is identified with quenched-in dislocations [45] together with residual stresses [49] at very low plastic strain levels. As deformation progresses towards stage II a few long, narrow dislocation walls start to occur and get well defined (2% strain) [45]. In this stage, dislocation density is found in a low magnitude inside ferrite. As deformation continues, dislocation density starts to raise, and inchoative dislocation cells become to develop and distribute into ferrite phase. Later on with more strain (>2%) in stage III, well-developed cell structure is observed predominantly in the ferrite. Moreover, the cell sizes did not change at higher strains (7% and 14%). However they tend to become thinner and well defined as further dislocations pack more inside the cell walls with increasing strain [45]. Figure 13 shows the microstructure of a DP steel reported by Korzekwa et al. [45] during stage II and stage III with respect to strain levels.

According to Gau and Huang [50], GNDs act as an obstacle against the statistically stored dislocations (SSDs) and do not assist in the plastic strain. SSDs are the types of dislocations which are accumulated without a geometrical consequence. According to Kocks [51], they are piled up by the statistical trapping of dislocations under plastic slip. The characterization of the GNDs is still in a deep discussion [52–54] due to the critical issue of strain dependence separately on GNDs or SSDs. Gau and Huang [50], also implied the importance of the separate identification of the SSDs and the GNDs. Many of strategies are available to calculate dislocation densities. Calcagnotto et al. [48] calculated dislocation densities of a DP microstructure with KAM, as mentioned and illustrated before in Figure 12 (b).

Measurements of Calcagnotto et al. [48] in GND densities of a DP microstructure matches up with the work of Sarosiek and Owen, [44] based on transmission electron microscope (TEM) studies of dislocation density measurements.

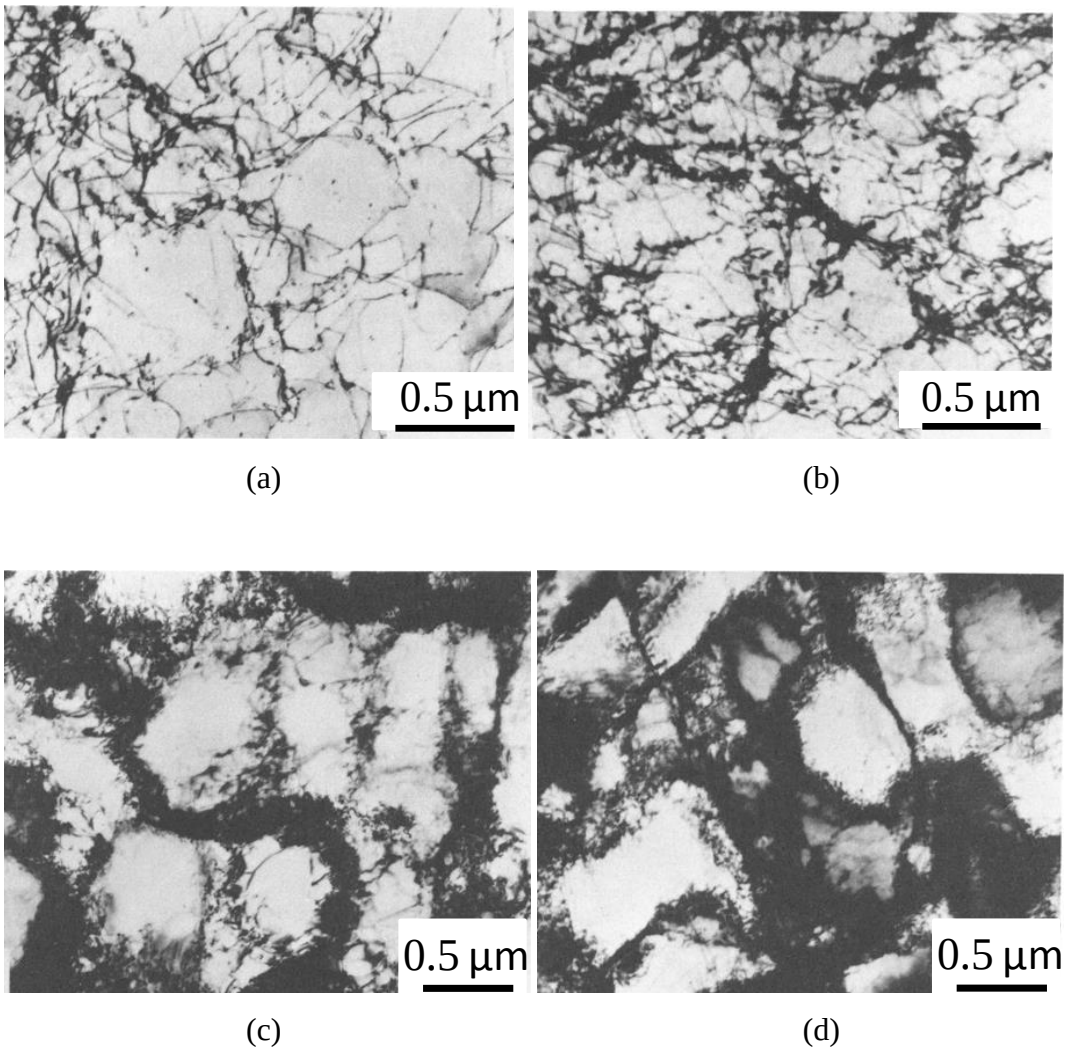

Figure 13 (a) Substructure in the DP steel, 1% strain (Stage II), (b) Substructure in the DP steel, 2% strain (Stage II), (c) Substructure in the DP steel, 7% strain (Stage III), (d) Substructure in the DP steel, 14% strain (Stage III) [45]

However, Calcagnotto et al., [48] reported in their work that some dislocation density measurements based on TEM studies [55,56] yield to a higher value of measured dislocation densities and these measurements do not overlap with their work [48].

Calcagnotto et al. [48] link this mismatch of calculated values with the argument due to the addition of SSDs while TEM observations. Gardner et al. [57] also performed a high-resolution electron backscatter diffraction (EBSD) on surface dislocation densities of polycrystals. There is also a method by using X-ray peaks to estimate dislocation density based on the materials strain and size contributions called as the modified Warren-Averbach [58] technique which is also used in this study and which will be detailed in the later sections.

2.4 Dynamic Strain Aging in Steels

The yield point phenomenon happening due to locking and unlocking of dislocations is a well-known phenomenon for mild steels [59,60]. In a tensile test, if a specimen is taken to the plastic regime under stress, and then unloaded by a following temperature-time treatment, C solute (Cottrell) atmosphere would form around the dislocations due to diffusion [60]. Reloading the specimen again results in gaining a new yield point which is higher than the one observed before but with a loss of ductility. This appearance of yield point is called as static strain aging. Static strain aging is aging while straining, gaining a higher yield point or yielding discontinuously.

When being influenced by high strain rates during tensile stress, the dislocations move fast but the solutes may not be able to catch the dislocations. As a result no aging will occur. Under same conditions with low strain rates, the solutes move fast yet the dislocation velocity might not be enough to catch them. Furthermore, test temperature could also affect as parallel as the strain rate. Under the test conditions of high temperature, the solute diffusion may be faster than the dislocation movement. Therefore, dislocations and the solutes could not encounter, as a result no aging will happen. Low temperature testing conditions may also lower down the diffusion speed of solutes. As a result aging could not be seen. Thus, continuous aging in a dynamic condition, i.e. tensile test, forms in a range of temperature, strain and certain strain rates [61,62].

This aging gives a raise on stress for the dislocations to pass the locking. Due to the adiabatic heating associated with high strain rate [63–65] certain mixtures of strain rate and temperature may state optimum conditions for DSA to occur, during forming processes. Unlike static strain aging, locking and unlocking in dynamic strain aging happens in row after row followed by a relief of stress, after some work hardening with some strain and gives a raise to the load drop. Any conditions that prevent an unstable flow behavior like DSA should be avoided during forming applications.

DSA shows up as serrated curves or jerky flow on the stress-strain curves. This jerky-serrated effect was first observed by Le Chatelier,(1909) while working on the flow curves of mild steels and in later years together with Portevin in an aluminum alloy [66]. Thereupon it is called as Portevin-Le Chatelier effect (PLC effect).

DSA in various kinds of steels has been a curious task for many researchers. Many grades of steels susceptible to DSA have been studied so far. Sachdev [26] worked on DP, HSLA and 1008 steels to enlarge the available knowledge of DSA effects on mechanical forming of these steels. Taheri et al. [67] studied on the drawability of the low C steel wire rods and reported the susceptible conditions which initiate strain aging. Verma et al. [68] reported DSA triggering conditions of a 9Cr1Mo grade steel also supported with some observations of dislocation substructures like bowing, kinking and loop formation occurring in the DSA region. On the twinning-induced plasticity steels (TWIP), DSA origination is studied in detail by Lee et al. [69]. As a result it is linked to reorientation in the C-Mn complex. Studies could be cited in many numbers similar to these pointed titles on DSA.

2.4.1 Dynamic Strain Aging in DP Steels

Same as other grades of steels, DSA can take place including the DP's, and increase strength and fatigue life at the expense of ductility and ductile-to-brittle transition temperature [26,70]. During DSA, solute atoms migrate into dislocation cores and cause a drop in the dislocation velocity by generating a dragging force [71]. Dislocations move freely when they overcome the dragging force, but the DSA process repeats once solute atoms catch the dislocations. The simultaneous straining and aging leads to the serrations in the stress-strain curves and disturbs the work hardening capability of the steel by increase of strength and decrease of ductility [33]. DSA dictation is reported between 250 – 400 ºC [25]., detected A sudden ductility drop in the DSA temperature range of DP steels is prescribed by Shahriary et al. [72]. Queiroz et al. [19], indicated that dynamic strain aging influences the mechanical properties starting from relatively low strain rates ($10^{-4}s^{-1}$, 10^{-3} s^{-1}, 10^{-2} s^{-1}) and high temperatures (25ºC-600ºC) mostly, and suggested that DSA is controlled by the locking of carbon atoms in the ferrite by distinguishing calculated activation energies at the beginning and at the end of the DSA behavior.

Some prevention applications are alloying, lowering the carbon content of the steel, carbide precipitating, and reduced forming in industrial applications. Alloying elements are added on the purpose of precipitating carbides to bond the interstitial free carbons. Therefore, the free carbon solute fraction is lowered to prevent possible DSA encounter. However, this method could cause unpredicted encountering of DSA in a period of time due to the dissolved carbons from carbides. Same as alloying, carbon content lowering and carbide precipitating are implemented methods to decrease the amount of free carbon of the steel. However, these methods are not reliable in a long usage time, especially for the use of these steels at high temperatures in applications. Thus, the first method to prevent DSA should be not passing into the DSA zone.

Since lightweight manufacturing is the main goal of the industry, replacing steel components with lightweight alloys and composite materials have become a mission nowadays. However, steels are still irreplaceable at some applications, especially in components working under dynamic conditions. Therefore, the only method of light-weighting on essential steel components is lowering the thickness of the component. Automotive industry, for example, establishes components of DP structures thicker than 1mm. Therefore the DP sheets could be assumed in plane-stress condition. As a result, the steel would struggle more amount of force concentrated in a reduced area. Thus, the steel has to show improved mechanical properties to survive. DP steels are an example of these kind of steels demonstrating high mechanical properties.

Considering DP steels, there is no record of thickness having a microstructural or a mechanical effect on DSA. However, in very thick applications, DSA occurrence could lead rupture or failure of the material in forming applications. Therefore, increasing thickness reduction increases the threat of DSA.

2.4.2 Symptoms of Dynamic Strain Aging

The serrated-jerky flow behavior is the most obvious discovered symptom of DSA. Besides serrations, some other mechanical properties like yield strength, strain hardening rate, ductility and strain rate sensitivity are showed as other symptoms of DSA [73]. Some uncommon behaviors like a peak in yield strength, a hollow of ductility or a negative strain rate sensitivity (NSRS) are reported in the work of Rodriguez [73] to be in a possibility of occurrence in the DSA zone.

In applications of metal forming, along with temperature, strain rate is probably the most important parameter among all. An unstable plastic flow can be recorded in a forming process of a material which shows NSRS. Since NSRS is known as one of the symptoms of DSA [73–76], during forming processes it can dictate the deformation process of the material. To prevent deterioration of the forming process, DSA should be avoided.

Due to the DSA, five types of serrations are identified in Figure 14 [73]. The well documented and the most famous types are type A, B and C. Type A reveals itself in a low temperature condition with an accompanying low strain rate. These serrations initiate at the same end of the specimen spread through the same direction [73]. Type B also occurs at high temperatures with low magnitudes of strain rates. This type of serrations occurs in a quick sequence due to the discontinuous band propagation. Type C serrations also occur at high temperatures with low strain rates though type C represents yield drops that occur below the trend of the stress-strain curves' extrapolation. Due to the yield drops, this type of serrations is thought to be seen due to the dislocation unlocking [73]. Type A serrations, convert into E types of serrations at high stain rates [73] under high temperatures. The type of serrations seen in the experimental results of this study are A and E on DP590 and DP800 steels, however, it is not discussed beside the mark of this study.

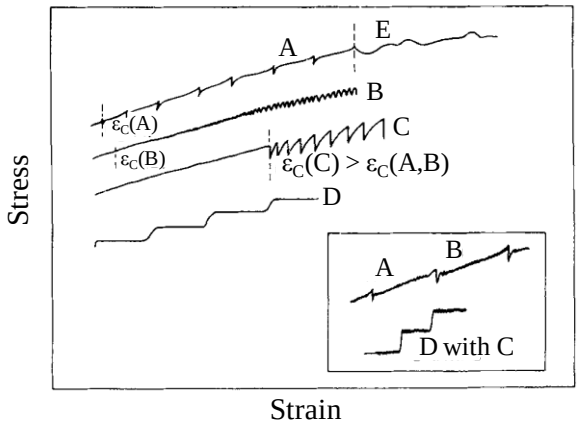

Figure 14 Types of serrations [73]

Grain size influence is also a considering fact on DSA. Between the range of 523-923 K a studied work on 316 grade of stainless steels with two different grain sizes (0.04-0.125 mm) illustrates the effect of grain size on DSA besides defining the serration types (Figure 15) [77].

Shifting of the DSA region to higher temperatures with increasing grain size is clearly seen in Figure 15. Under DSA conditions, smaller grain size establishes suitable conditions for strong pinning and accordingly the most rapid and strongest dislocation immobilization. Strain hardening increase with decreasing grain size in inevitable. Therefore DSA peaks of serrations become sharper with decreasing grain sizes.

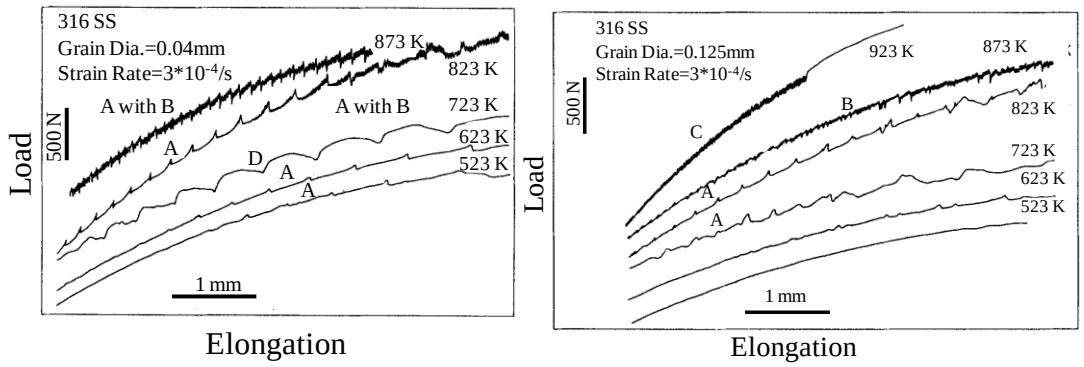

Figure 15 Evolution of DSA comparing with grain size [77]

2.5 Main Findings and Gaps in the Literature

As mentioned before, steels like low carbon ferritic-pearlitic, bake-hardenable, HSLA etc. are systematically studied considering microstructural and thermomechanical features. However, current studies on DP steels are mostly focused on crash (high strain rates) and quasi-static deformation behavior (low strain rates). Due to their significant area of usage on the critical parts of specific industrial applications, a systematical study on thermomechanical forming conditions of DP steels is essential.

Since DSA is a threat to forming, an extensive work on relative thermomechanical conditions is a necessity. DSA can decrease the strain hardening exponent and the strain rate sensitivity, which may cause deterioration on forming.

Moreover, DSA in DP steels could be more complicated than low carbon ferritic and pearlitic steels due to the existence of the dual-phase microstructure of ferrite and martensite. The volumetric fractions of each phase and morphology of the structure may have significant effects on the DSA mechanisms which are not fully explained in the current literature.

CHAPTER 3

MATERIALS AND METHODS

The 2-mm-thick DP590 and DP800 steel sheets were supplied from Swedish Steel Works, SSAB and their chemical compositions are listed in Table 3. Microstructure of both materials was examined by optical microscopy after the metallographic preparation and %2 Nital swab for 2 seconds. This reagent faded out the martensite. Thus it was possible to visualize each phase, seen in Figure 16. The fraction of each phase and the mean grain sizes were measured by Adobe Photoshop and Huvitz HDS-5800 Digital Microscope Software. The DP590 contained 83% ferrite with 9.3 ± 2.5 μm grain size and DP800 contained 62% ferrite with 8.7 ± 2.1 μm grain size.

Table 3 Chemical compositions of the investigated grades

Mass Contents (%)	C	Si	Mn	P	S	Cr	Mo	Ni	Cu	Al	Fe
DP590	0.081	0.284	1.517	0.008	0.004	0.02	0.006	0.033	0.015	0.038	97.90
DP800	0.12	0.194	1.549	0.007	0.002	0.035	0.009	0.025	0.011	0.032	97.89

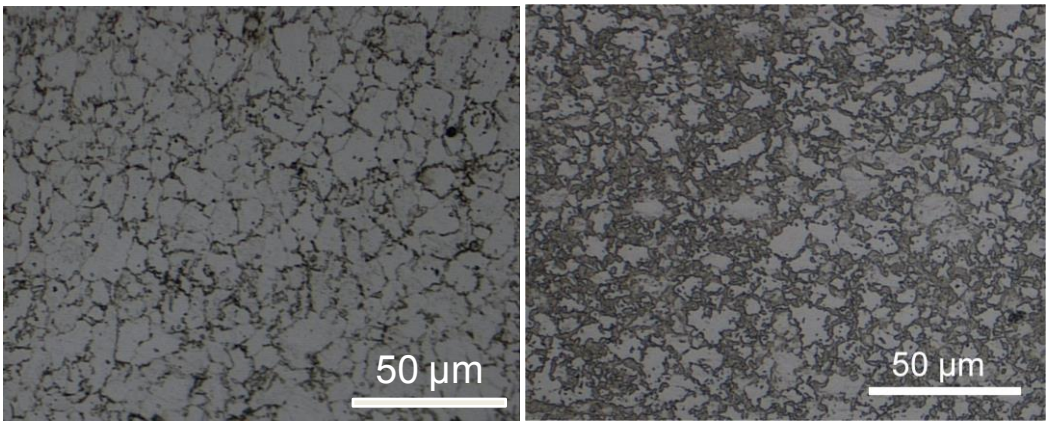

(a) (b)

Figure 16 Microstructures of DP590 (a) and DP800 (b)

The mechanical properties of both steels were confirmed by tensile testing according to the ASTM E-8 standard. Dog-bone shaped specimens were cut off by electrical discharge machining (EDM) in the angles 0^o, 45^o, 90^o with respect to the rolling direction. Overall, 5 tests were performed under room temperature at 1mm/min extension rate for each condition using a Zwick Z250 universal testing machine. Figure 17 shows the representative stress-strain curves of DP590 and DP800 steels along the rolling direction. The general mechanical properties were obtained from these curves.

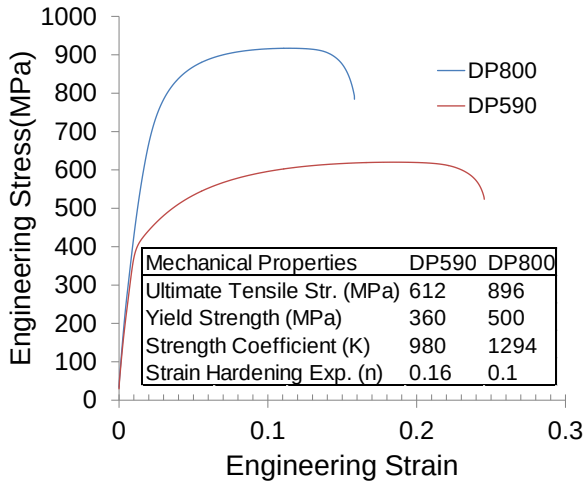

Figure 17 Representative stress-strain curves of DP590 and DP800

The constant (true) strain rate and high temperature tests were performed on a deformation dilatometer (TA-BAEHR DIL805T, Figure 18) in the rolling direction of both steels. The tests are conducted under true strain rate control using the close-loop mechanical control of the test system. However, to evaluate tensile stress, uniform and total strains, collected data were converted to engineering stresses and strains and represented as such. The strain hardening exponent, strength coefficient and strain rate sensitivity values, on the other hand, were calculated from the native true stress-strain data. The samples were manufactured by EDM and had features and dimensions shown in Figure 19. An induction coil heated the samples during testing at a rate of $100^oC/s$ to avoid microstructural changes and relaxation.

Figure 18 TA-BAEHR DIL805T deformation dilatometer

During the tests, the specimens were continuously cooled using pressurized helium gas at a constant flow rate to minimize deformation heating while the closed-loop thermal control system maintained the temperature within 5^{o}C during the tests using by adapting the power delivered to the induction coil. Overall, a minimum of 2 tests were performed at 25^{o}C (RT), 100^{o}C, 200^{o}C, 300^{o}C, 400^{o}C and 10^{-3} s^{-1}, 10^{-2} s^{-1}, 10^{-1} s^{-1}, 1 s^{-1}. The load cell in the dilatometer recorded the stresses, and the strains were measured by a high resolution displacement transducer (LVDT).

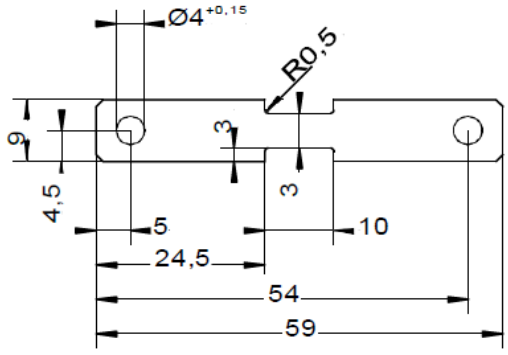

Figure 19 Technical drawing of the testing specimen used in the dilatometer (mm)

Dislocation densities in both grades in their as-received and deformed conditions were measured by X-Ray Diffraction Analysis (XRD). Diffraction data were collected by a Bruker D8 diffractometer operating with 40 kV - 40 mA, CuKα (λ= 0.154 nm) source at a 40^o-90^o angle, 0.1^o/ minute ratio. The data was later processed by XPowder12 [78] software utilizing the modified Warren-Averbach analysis [58]. In the current study, dislocation density measurements were all performed by the modified Warren-Averbach analysis on DP590 and DP800. XRD analysis of DP590 sheet steel were performed on steel samples which are strained at different levels, 0%, 12%, respectively. Through XRD analysis, dislocation densities of each strained sample were evaluated from the modified Warren-Averbach analysis. The reason for focusing on DP590 is the visible jerky flow-serrations on the stress-strain curves of DP590 samples. DSA also exists in DP800, yet it is not clearly visualized in the stress-strain curves. Therefore the discussion of this concept is just studied on DP590 samples. Meanwhile, the dislocation density of DP800 at 0% strain condition was also calculated to support the suggested model later in this study.

In this analysis, the diffraction peaks are converted to a Fourier form, and the real part of the Fourier coefficients is given as:

$$lnA(L) = lnA^S(L) - \rho\frac{\pi b^2}{2}L^2 ln\left(\frac{R_e}{L}\right)\left(K^2\overline{C}\right) + Q(K^4\overline{C}^2) \quad (1)$$

where $A^S(L)$ term contains the size and the rest contains the distortion (strain) effects. L is the Fourier length, ρ is the dislocation density, b is burgers vector, R_e is the effective cut-off radius, $K = 2\sin\theta/\lambda$, $\overline{C}$ is the average contract factor of the dislocations and defined as:

$$\overline{C}_{hkl} = \overline{C}_{h00}(1 - qH^2) \quad (2)$$

While it is possible to determine q experimentally from a modified Williamson-Hall analysis [79], we assumed the following constants, $\overline{C}_{h00}$ = 0.32 and q = 2.07, for the ferrite by taking the average of values reported in [79] for edge and screw dislocations in the bcc materials. H^2 is also given in [79] as:

$$H^2 = (h^2k^2 + h^2l^2 + k^2l^2)/(h^2 + k^2 + l^2)^2 \quad (3)$$

where *h*, *k*, *l* are the Miller's indices of each peak.

The size term, $A^S(L)$, in Equation 1 can be obtained from a *lnA(L)* vs. $K^2\overline{C}$ plot using various L values, when $K^2\overline{C}$ = 0. Instead, we obtained the size coefficient and the *lnA(L)* directly from the XPowder12 software. By neglecting the higher order terms in Equation 1, the dislocation density can be obtained from the following relationship:

$$\frac{lnA(L) - lnA^S(L)}{(K^2\overline{C})L^2} = \rho\frac{\pi b^2}{2}lnR_e - \rho\frac{\pi b^2}{2}lnL. \quad (4)$$

For a given peak, the $K^2\overline{C}$ term is constant. Then, the Fourier coefficients and the $K^2\overline{C}$ term can be merged into a single term, Y/L^2, which can be plotted versus *lnL*. The slope of this plot contains the dislocation density. Figure 20 shows the diffraction peaks of the DP590 and DP800 sheet samples collected from X-ray analysis in different strain conditions. Note that the peaks of the (220), (310), (222) crystallographic planes are not discussed.

The modified Warren-Averbach technique also does not give the calculation of dislocation densities in each phases separately. The reason of this overlap on the peaks of martensite and ferrite on the same peaks could be body centered phase structure common in two phases (with only "c" dimension different in martensite). The correction of our measurements were done by correlating with the past works done on TEM [56] and EBSD [47] measurements and found to be fine to use in our calculations.

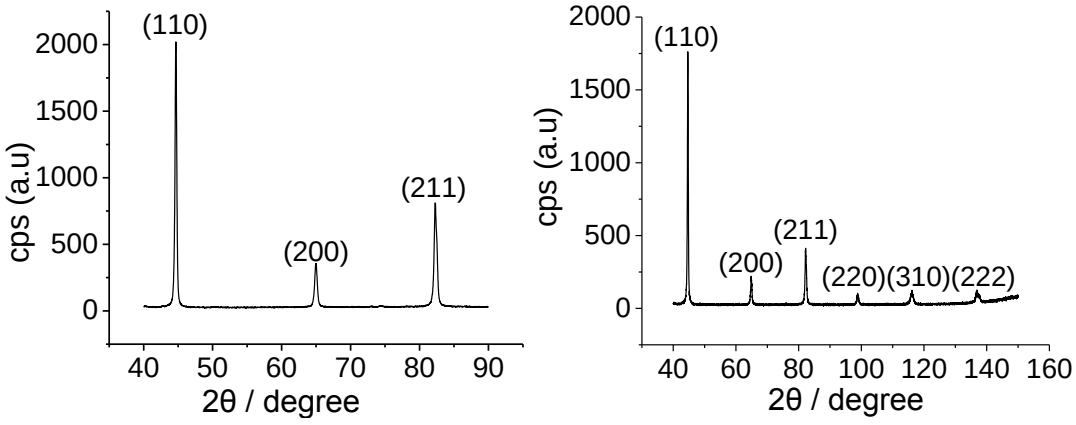

(a) (b)

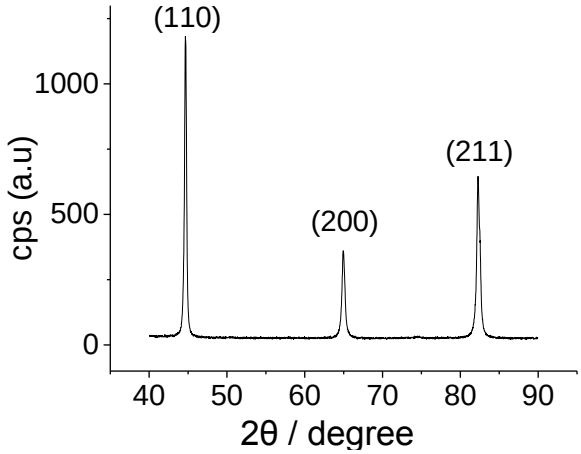

(c)

Figure 20 X-ray diffraction data in different strained conditions (a) (110), (200), (211) crystallographic planes for DP590 0% strain, (b) (110), (200), (211) (220), (310), (222) crystallographic planes for DP590 12% strain, (c) (110), (200), (211) crystallographic planes for DP800 0% strain

The analysis of the Fourier forms of these peaks resulted in errors which cannot be disregarded. The reason of these errors is the small size of peaks. The same situation was also reported by Shintani and Murata [80] on X-ray analysis of an austenitic stainless steel.

Therefore only first three peaks belong to the crystallographic planes (110), (200) and (211) were taken into account for the modified Warren-Averbach analysis.

Table 4 Real part Fourier and size values from Fourier form of DP590 0% strain

DP590 (0%)				
Fourier Coef.	**Real Part & Size**	**2-Theta(degree)**		
		45°	**65°**	**82°**
L=20	**A(L)**	0.34	0.36	0.27
L=15		0.51	0.54	0.43
L=10		0.71	0.74	0.68
L=20	**A_s(L)**	0.36	0.36	0.36
L=15		0.54	0.54	0.54
L=10		0.74	0.74	0.74
L=20	**lnA(L)**	-1.0788097	-1.0216512	-1.3093333
L=15		-0.6733446	-0.6161861	-0.8439701
L=10		-0.3424903	-0.3011051	-0.3856625
L=20	**lnA_s(L)**	-1.0216512	-1.0216512	-1.0216512
L=15		-0.6161861	-0.6161861	-0.6161861
L=10		-0.3011051	-0.3011051	-0.3011051

The real part Fourier and size data acquired from the Fourier forms for the peaks 45°, 65° and 82° of the dual phase sheets in different strained conditions are given in Table 4, Table 5 and Table 6 for each DP590 0% strain, DP590 12% strain and DP800 0% strain, respectively. By combining together in Equation 4 with the data given in Table 7, Y/L^2 vs lnL plot for random Fourier lengths (L=20, 15, 10) gives the dislocation density for each sample. Y/L^2 vs lnL plot for the strongest intensity (110) peak gives the dislocation density of DP590 0% strain as 3.1 x 10^{14} m^{-2}, DP590 12% strain as 4.2 x 10^{14} m^{-2}, DP800 0% strain as 6.3 x 10^{14} m^{-2}, in Figure 21 for each. For the (200) and (211) peaks, the dislocation density and the error in the calculations increase by 50% for all samples. Therefore (110) peak throughout this study for the dislocation density measurements is only used.

Table 5 Real part Fourier and size values from Fourier form of DP590 12% strain

DP590 (12%)				
Fourier Coef.	**Real Part & Size**	**2-Theta(degree)**		
		45°	**65°**	**82°**
L=20	**A(L)**	0.26	0.37	0.13
L=15		0.44	0.55	0.3
L=10		0.71	0.8	0.61
L=20	**A_s(L)**	0.37	0.37	0.37
L=15		0.55	0.55	0.55
L=10		0.8	0.8	0.8
L=20	**lnA(L)**	-1.3470736	-0.9942523	-2.0402208
L=15		-0.8209806	-0.597837	-1.2039728
L=10		-0.3424903	-0.2231436	-0.4942963
L=20	**lnA_s(L)**	-0.9942523	-0.9942523	-0.9942523
L=15		-0.597837	-0.597837	-0.597837
L=10		-0.2231436	-0.2231436	-0.2231436

Table 6 Real part Fourier and size values from Fourier form of DP800 0% strain

DP800 (0%)				
Fourier Coef.	**Real Part & Size**	**2-Theta(degree)**		
		45°	**65°**	**82°**
L=20	**A(L)**	0.22	0.29	0.11
L=15		0.37	0.46	0.22
L=10		0.6	0.68	0.47
L=20	**A_s(L)**	0.29	0.29	0.29
L=15		0.46	0.46	0.46
L=10		0.68	0.68	0.68
L=20	**lnA(L)**	-1.5141277	-1.2378744	-2.2072749
L=15		-0.9942523	-0.7765288	-1.5141277
L=10		-0.5108256	-0.3856625	-0.7550226
L=20	**lnA_s(L)**	-1.2378744	-1.2378744	-1.2378744
L=15		-0.7765288	-0.7765288	-0.7765288
L=10		-0.3856625	-0.3856625	-0.3856625

Table 7 Average contrast factor, H^2 and $\left(K^2\overline{C}\right)$ of the analyzed peaks

	2-Theta(degree)		
	45°	**65°**	**82°**
$\overline{C}$	0.15	0.32	0.15
$\mathbf{H^2}$	0.25	0	0.25
$\mathbf{K^2\overline{C}}$	12.50 nm^{-2}	41.56 nm^{-2}	24.84 nm^{-2}

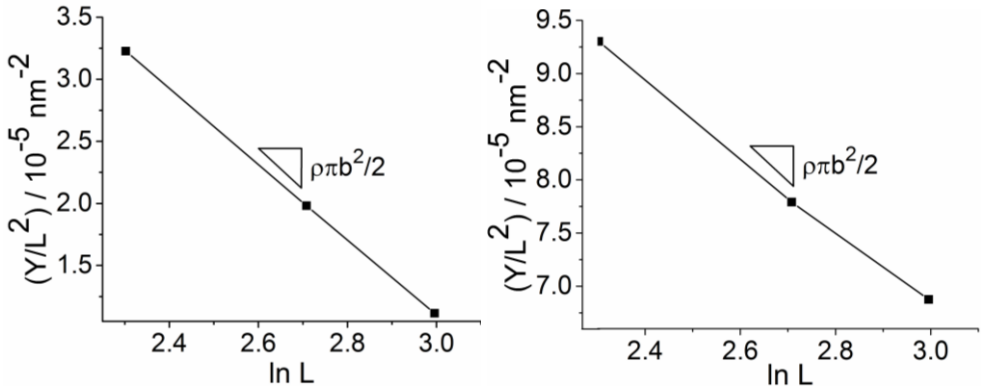

(a) (b)

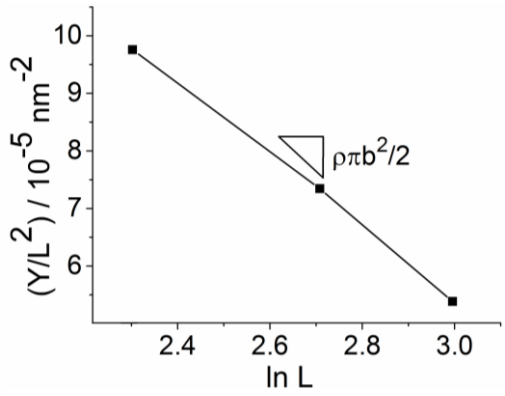

(c)

Figure 21 *Y/L*^{2} versus *lnL* plot for the dislocation density calculations (a) DP590 0% strain (b) DP590 12% strain (c) DP800 0% strain

CHAPTER 4

RESULTS AND DISCUSSION

4.1 Mechanical Properties at the Intermediate Strain Rates and Temperatures

4.1.1 Mechanical Properties of DP590

Figure 22 shows the temperature effects on the mechanical behavior of DP590 at an intermediate strain rate of 0.01 s^{-1}. The common expectation is a softening and a gain in ductility with increasing temperature. While this is true at 100^{o}C and 400^{o}C, the trend is reversed at 200^{o}C and 300^{o}C. There is a resistance to thermal softening between 200 and 300^{o}C, accompanied by the ductility loss. The strength of the material at 300^{o}C is significantly more than the ones tested at 100^{0}C and 200^{o}C. There is almost no thermal softening at 300^{o}C and the high temperature strength is similar to the one at room temperature. Under these conditions, DP590 showed indications of dynamic strain aging behavior, which is characterized by the discontinuous plastic flow (serrations). The serrations are more distinct at 200^{o}C, yet it is also visible also at 300^{o}C, indicating the DSA dominant deformation in this temperature range.

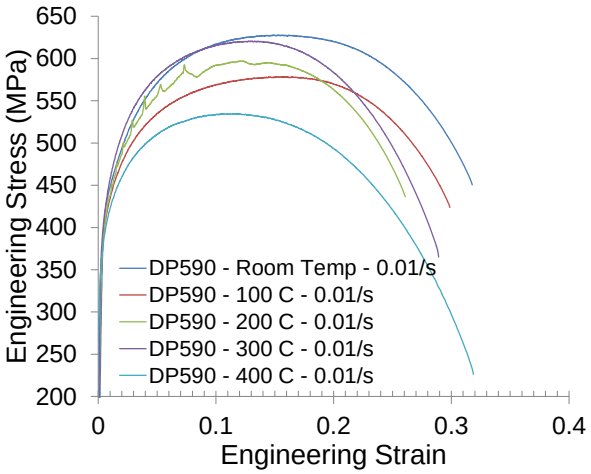

Figure 22 Stress-strain curves of DP590 between room temperature - 400°C at a constant strain rate of $0.01s^{-1}$.

To confirm the lack of DSA at RT and 400°C, DP590 is tested at various strain rates under constant temperature (Figure 23). The effects of strain rate under RT and 400°C were as expected. With increasing strain rates, the corresponding UTS increases and the overall ductility drops and these results are parallel to the literature [22,81]. Except the tiny serrations at 400°C - $0.001s^{-1}$, there are no visible serrations in the stress-strain curves. At all strain rates, there is significant softening in DP590 when heated to 400°C. This softening, however, does not seem to increase the ductility and may even cause a loss of uniform elongation (RT - $0.001s^{-1}$ vs 400°C - $0.001s^{-1}$).

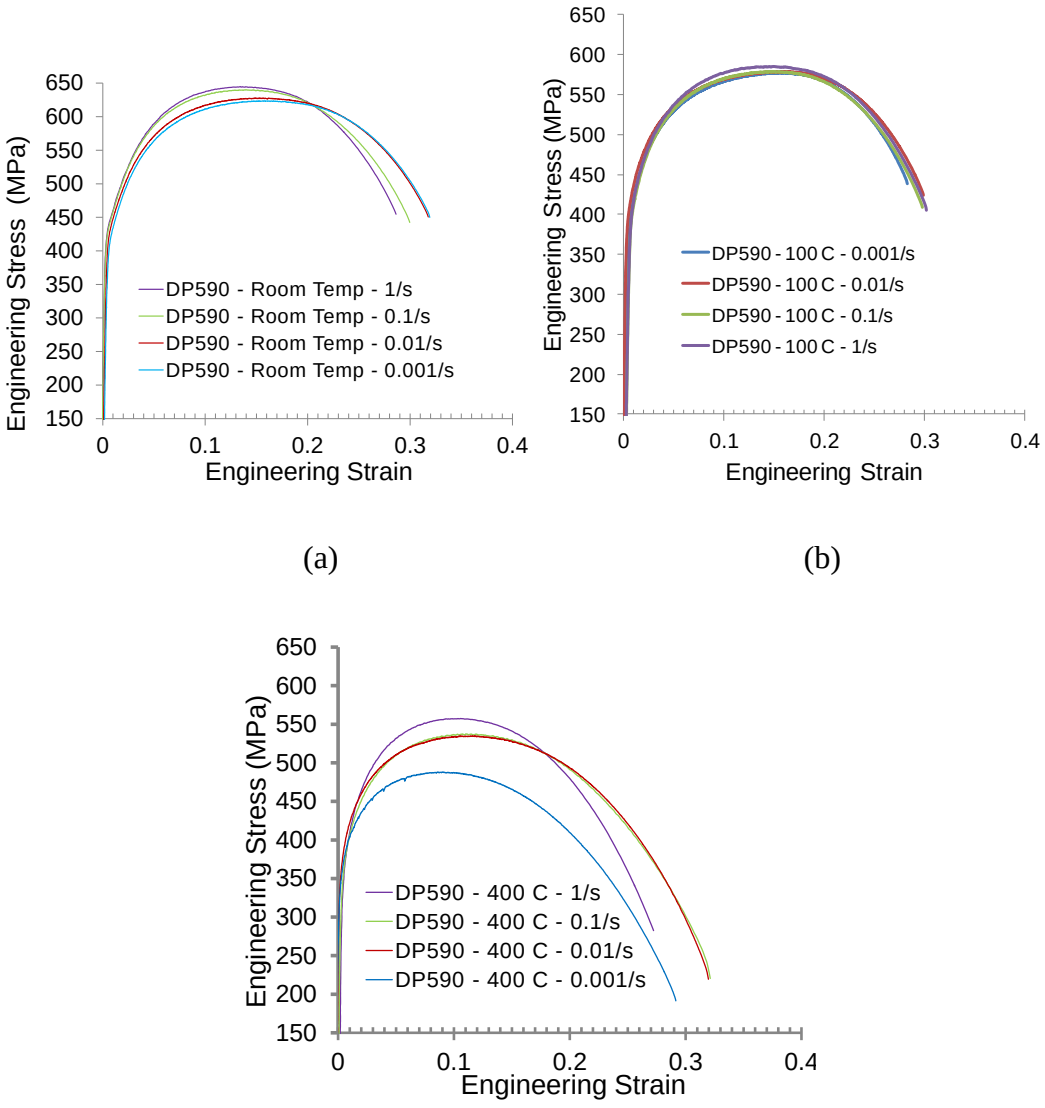

Figure 23 Stress-strain curves of DP 590 (a) under room temperature, (b) 100^{o}C and (c) 400^{o}C at different strain rates.

On the other hand, abnormal deformation behavior is observed when the DP590 is tested at various strain rates at the constant temperatures of 200^{o}C and 300^{o}C (Figure 24). The DP 590 softens, yet it loses significant ductility with increasing strain rates at these temperatures.

Serrations accompany the stress-strain curves at almost all strain rates, while they are the most distinct at T=200°C, $\dot{\varepsilon}$ =0.01s^{-1} and 0.1s^{-1}, and they gradually disappear with increasing strain rate (1s^{-1}). As the temperature increases to 300°C, the serrations are clearly visible at $\dot{\varepsilon}$ = 0.1s^{-1} and 1 s^{-1}, and disappears at the lower strain rates, $\dot{\varepsilon}$ =0.01s^{-1} and $\dot{\varepsilon}$ =0.001s^{-1}. When compared to the results at 200°C, the frequency and magnitude of the serrations appear to be lower at 300°C. With the increasing temperatures, intense serrations also shift toward to higher strain rates.

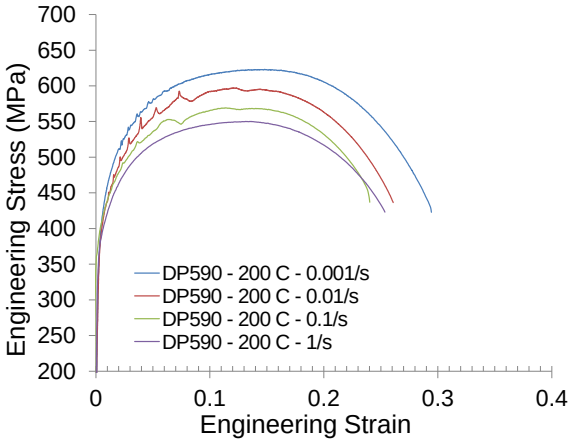

(a)

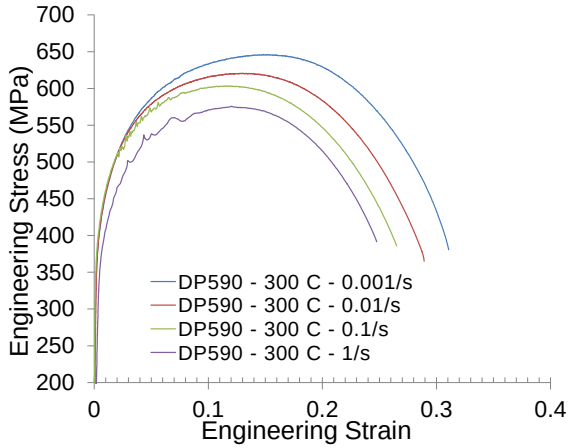

(b)

Figure 24 Stress-strain curves of DP 590 under (a) 200°C and (b) 300°C at different strain rates.

Our results indicate that the DSA controls the deformation in a specific and narrow temperature range (200°C - 300°C). Queiroz et al. [19] observed a similar range in DP590 low strain rates. The abnormal behavior and the serrations observed in this study at higher rates confirm that the DSA might exist within a range of strain rates. The resistance to thermal softening is evident at all strain rates for 200°C and 300°C (Figure 25(a)). At $\dot{\varepsilon} = 0.001 s^{-1}$, the strength becomes equal or even higher than the room temperature. The serrations are minimal at this strain rate, yet the effects of DSA are the most significant. The opposite is true for the ductility. The effects of the DSA become most severe and detrimental at higher strain rates. As shown in Figure 25(b) the total strain decreases from ~ 0.3 to ~ 0.2 between 0.1 and 1 s^{-1} at both 200°C and 300°C. In this case, there is a correlation between the ductility and the serrations in the flow behavior. The ductility loss is most significant when there is an intense serration. Moreover, testing at 300°C results in the lowest ductility of 0.21. Indeed, within the DSA range ductility is always lower at higher temperatures. Ductility recovers to ~ 0.3 at 400°C and becomes independent from strain rate. Also at RT and 100°C, ductility is independent from the strain rate and has an average value of 0.3.

The clear negative strain rate sensitivity (NSRS) of the material is another interesting point of the material in the DSA region, which is also reported as a common symptom of DSA even serrations are not observed. Since NSRS causes unstable flow and localization, it may be responsible for the reduced ductility.

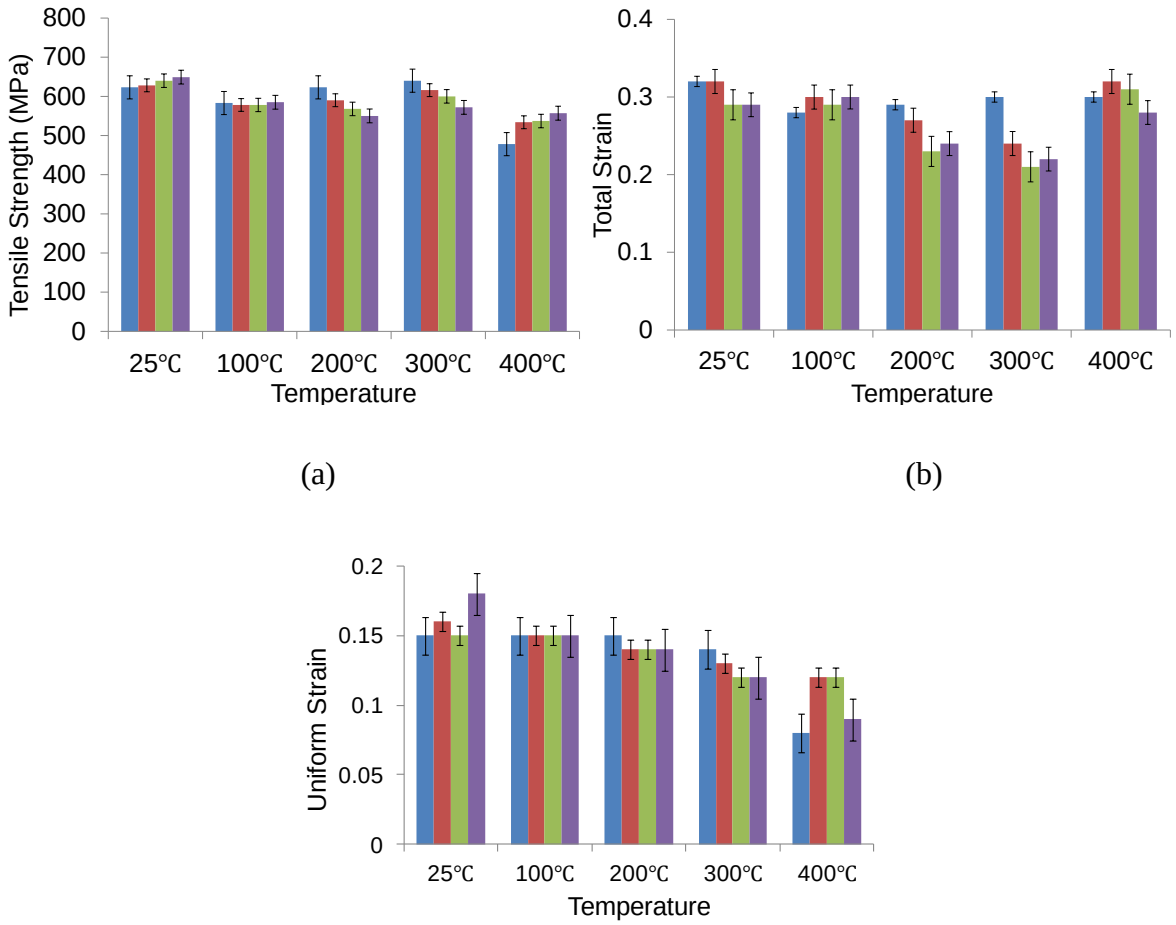

Figure 25 Comparison of (a) UTS, (b) Total Strain, (c) Uniform Strain of DP590 at all strain rates and temperatures. Blue, dark red, green and purple bars represent ἑ =0.001s^{-1}, ἑ =0.01s^{-1}, ἑ =0.1s^{-1}, ἑ =1s^{-1} respectively.

Figure 25(c) represents the uniform strain of DP590 under all conditions. Independent from the DSA, uniform strain decreases with increasing temperature at constant strain rate. However, the percent decrease is maximum at 400ºC, decreasing by almost 50% when compared to the room temperature values. Within the DSA range, uniform strains decrease by almost 30%, especially under the higher strain rates of 0.1 and 1 s^{-1}.

This loss of strain hardening capability at the higher rates also coincides with the loss in total ductility. Under different strain rates at constant temperature, the uniform strain of DP590 may be assumed steady. There is no significant change in the uniform elongation with increasing strain rate.

4.1.2 Mechanical Properties of DP800

DP800 softens with increasing temperature at a constant strain rate of 0.1 s^{-1} (Figure 26). This result is parallel to the work Khan et al., 2012 [82]. However, at 100^{o}C, 200^{o}C and 300^{0}C, the softening is minimal accompanied by a significant ductility loss. Only at 400^{o}C, there is thermal softening and a ductility increase. When tested under different strain rates, the mechanical behavior is in accordance with the literature for RT, 100^{o}C and 400^{o}C (Figure 27) [83]. This result is similar to DP590, under the same conditions except the slight difference seen on the strengthening behavior of DP800 under 100^{o}C with increasing strain rate. DP800 is more sensitive to change tendency towards NSRS at earlier temperatures (from RT to upper temperatures) compared to DP590. For all of these conditions, there is strengthening with the increasing strain rate. However, the ones under 200^{o}C and 300^{o}C display some abnormalities similar to the DP590. These results suggest that the DSA may control the mechanical behavior between 200^{o}C - 300^{o}C in DP800.

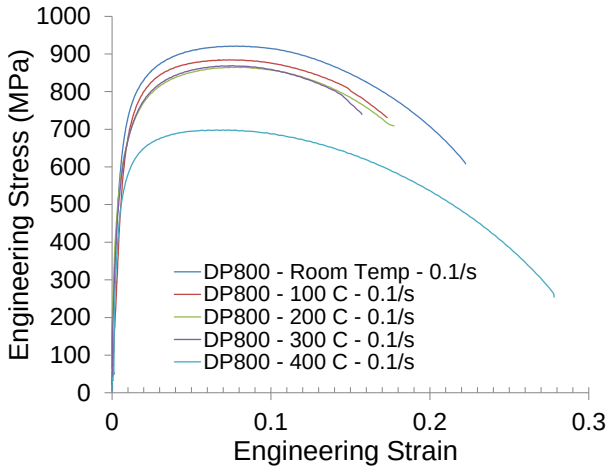

Figure 26 Stress-strain curves of DP800 between room temperature - 400^{o}C at a constant strain rate of 0.1s^{-1}.

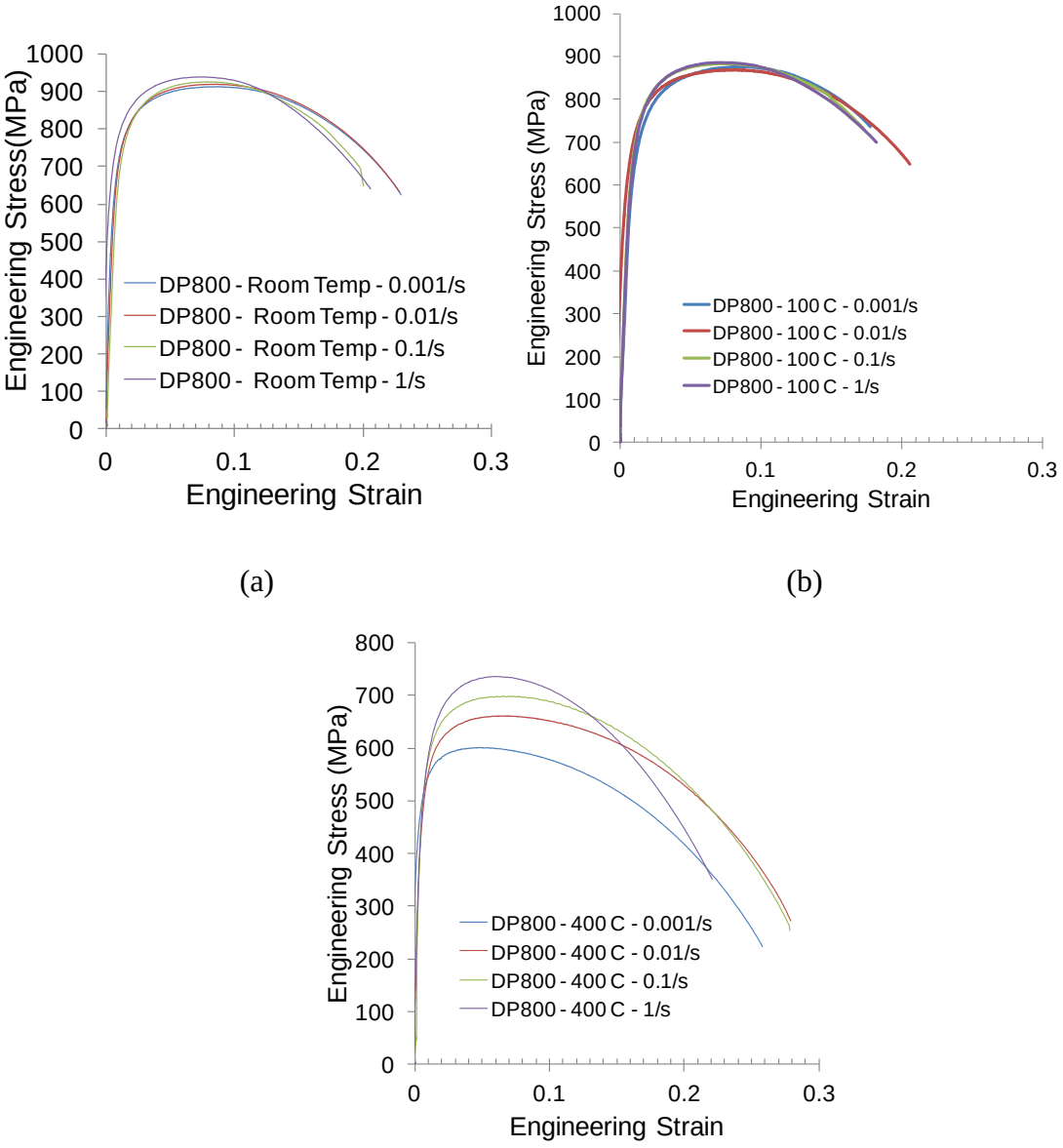

(a) (b)

(c)

Figure 27 Stress-strain curves of DP 800 (a) under room temperature, (b) 100^{o}C and (c) 400^{o}C at different strain rates.

Figure 28 shows the variation of stress-strain for the tests of DP800 performed at 200^{o}C and 300^{o}C, under different strain rates. Under these conditions, there are no serrations in the stress-strain curves, except the ones tested at $\dot{\varepsilon}$ =0.001s^{-1}. Yet, both the strength and ductility decrease with the increasing strain rate at 200^{o}C.

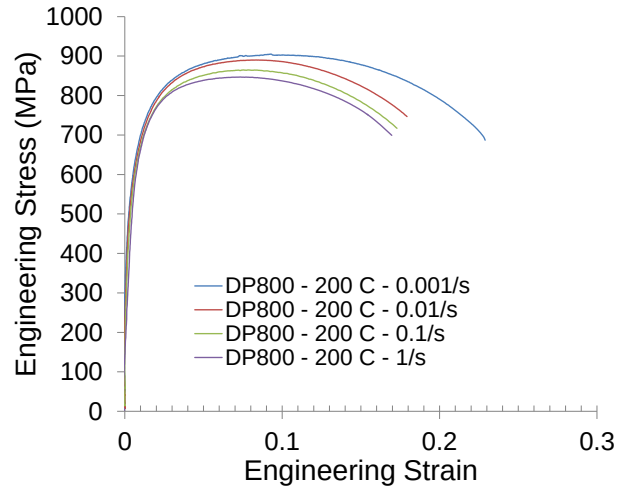

(a)

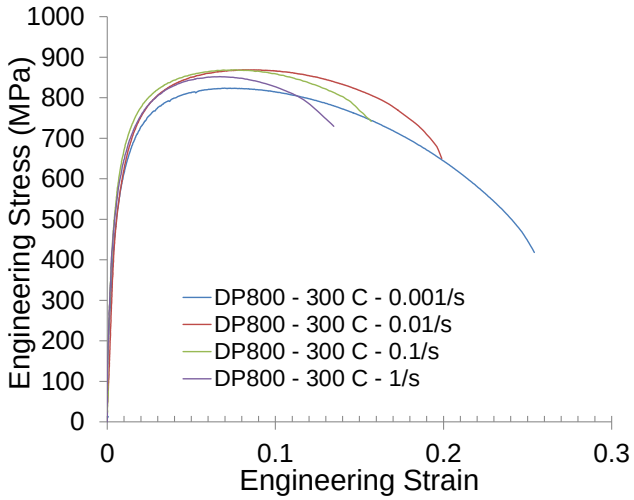

(b)

Figure 28 Stress-strain curves of DP800 under 200°C and 300°C at different strain rates.

The ductility loss is even worse at 300°C, with minimal strengthening with the increasing strain rate. Similar to DP590, the test at 200°C indicates NSRS clearly, which also support the presence of DSA.

Therefore, the lack of serrations in the stress-strain curves of DP800 does not change the abnormal mechanical behavior and still suggest a DSA-controlled mechanical behavior between 200^{o}C – 300^{o}C.

Figure 29(a) and 29(b) illustrating the strength and ductility of DP800 demonstrate the abnormal behavior within the DSA region. Resistance against thermal softening is evident at all strain rates. The strength remains almost unchanged until 300^{o}C, followed by up to 40% decrease at 400^{o}C. While the strength is steady within ± %5 margin at 200^{o}C and 300^{o}C, the increasing strain rate causes a significant drop in ductility. Similar to the DP590, the effects of DSA on the ductility are exacerbated at high temperatures and high strain rates. Tests at 300^{o}C and 1s^{-1} result in the lowest ductility of 0.13, which is a 35% decrease compared to the room temperature value. Ductility recovers back to 0.22 at 400^{o}C, without a meaningful change with the strain rate. Unlike the ductility, the uniform strain is almost independent of the strain rate at all temperatures (Figure 29(c)). The increase in temperature under constant strain rate, on the other hand, results in a slight decrease in the uniform strain until 400^{o}C. At 400^{o}C, the uniform strain decreases by 50% compared to the room temperature values. This is in parallel to the significant softening observed at this temperature.

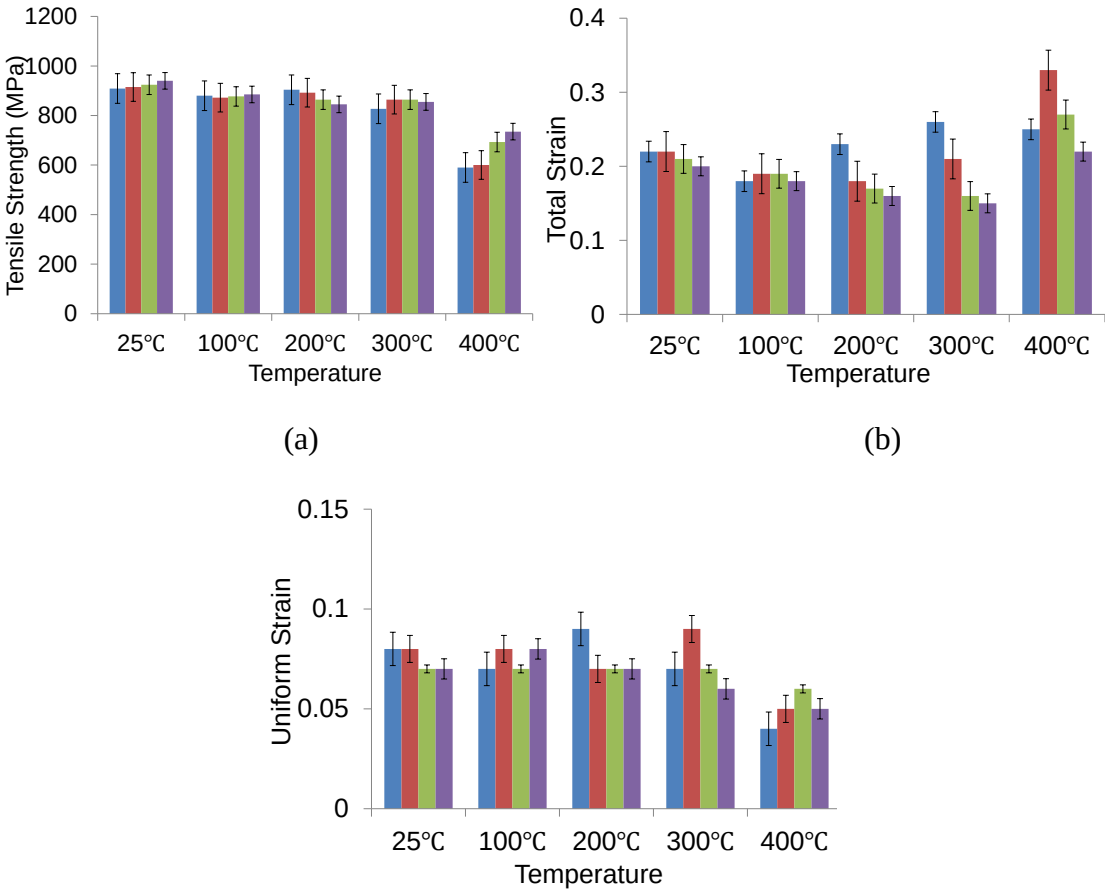

Figure 29 Comparison of (a) UTS, (b) Total Strain, (c) Uniform Strain of DP800 at all strain rates and temperatures. Blue, dark red, green and purple bars represent $\dot{\varepsilon}$ =0.001s^{-1}, $\dot{\varepsilon}$ =0.01s^{-1}, $\dot{\varepsilon}$ =0.1s^{-1}, $\dot{\varepsilon}$ =1s^{-1} respectively.

4.1.3 Comparison of DP590-DP800 and Implications for Formability

When compared to the room temperature results, both grades of steel soften when heated to 100°C or 400°C and display ordinary mechanical behavior (Figure 30). While the softening is minimal at 100°C (up to 10%), uniform and total ductility stay constant. There is a significant softening in both grades (especially for DP800) at 400°C, without a significant gain in ductility. The uniform strain decreases considerably at this temperature and may lead to early necking and plastic instabilities during forming.

Therefore, warm forming of these steels seems to be only feasible at 100ºC up to strain rates of 1 s^{-1}. When heated above 100ºC, both grades of steel exhibit abnormal mechanical behavior and this may result in a lower formability (Figure 30(a)).

DSA controlled deformation between 200ºC - 300ºC in DP590 is usually characterized by the serrations in the stress-strain curve, whereas they are mostly absent in DP800. Independent from the serrations, both steels show similar anomalies in their mechanical behavior. The effects of the DSA are most intense at 300ºC for DP590 and they are concentrated at 200ºC for DP800 (Figure 30). The differences in the microstructure can be a reason for the observed properties. The DP590 contains a higher amount ferrite phase (~ 83% ferrite) compared to the DP800 (~ 62%). It is assumed that during deformation, martensite stays with a fixed-high dislocation density and the deformation starts in ferrite which carries on with increasing dislocation density with respect to increasing strain [44]. As the DSA occurs due to the pinning of these mobile dislocations, the greater amount of ferrite is expected [48] to intensify the effects of DSA. In addition to the serrated stress-strain curves, the large variations in the properties of DP590 confirm the effects of ferrite on the DSA behavior. Both the strength and ductility become strain rate sensitive. When compared to DP590, DP800 also exhibit variation in the properties but to a smaller extent. Although serrations are absent in the stress - strain curves of DP800, DSA still results in the abnormal deformation around 200ºC.

There are two major effects of DSA in both materials (Figure 30). First, there is resistance to thermal softening within the DSA range and the strength has negative strain rate sensitivity. The NSRS values were calculated from the true stress-strain curves by; $m = \log(\Delta\sigma_{0.05}/\Delta\dot{\varepsilon})$. DP590 has m = -0.017 at 200ºC m = -0.006 at 300ºC and DP800 has m = -0.008 and m = 0.01, respectively. Second, the total and uniform ductility decrease simultaneously with increasing strain rates and temperatures. Combined with the NSRS, lower uniform strains at these conditions should result in poor formability. The plastic instabilities in the form of local necks may start early in the deformation, and the strain will accumulate in these instabilities due to the NSRS.

Therefore, temperatures between 200 - 300ºC should be avoided at any strain rate during forming of both grades. In our tests, these temperatures are obtained by preheating the samples. However, in real forming practice, the samples may reach these temperatures because deformation heating at high strain rates (10 – 100 s^{-1}) employed in industrial forming processes. As the strain rate gets higher (10 – 100 s^{-1}), the adiabatic heating may raise the local temperature of the deforming regions to the DSA range. The higher strain rates can also intensify the effects of DSA and result in a further reduction in the total ductility and the formability.

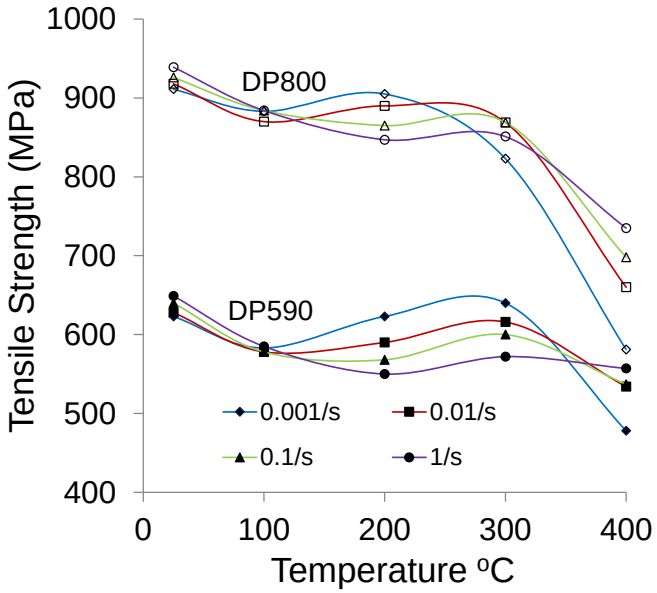

(a)

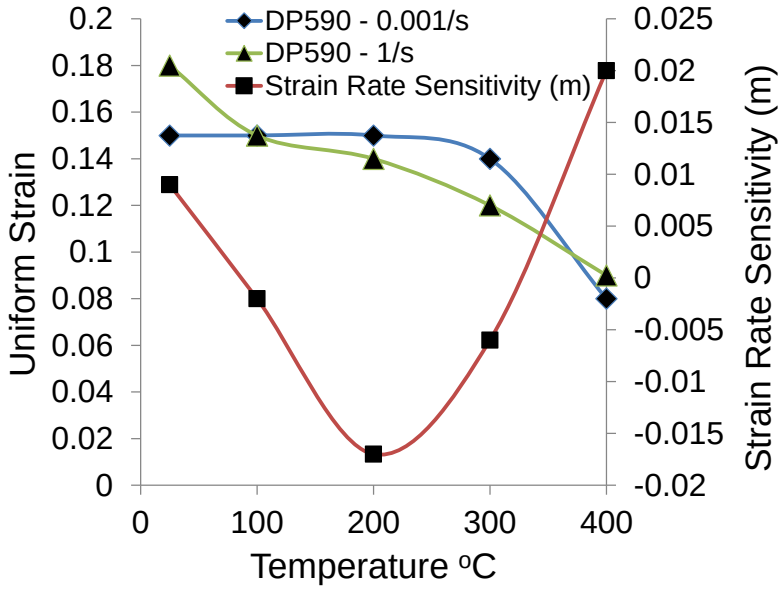

(b)

Figure 30 (a) Comparison of the mechanical behaviors of DP590 and DP800 and the DSA controlled deformation between 200°C – 300°C (b) Evolution of the uniform strain and the strain rate sensitivity with temperature in DP590.

4.2 Dynamic Strain Aging in DP steels

DSA happens due to the pinning of dislocations by the solute atoms. Once the dislocations break free from the pinning, the diffusion rate of the solute atoms will not be enough to catch the moving dislocations. Carbon atoms diffuse by only 4.8 x 10^{-9} μm ($x = \sqrt{Dt}$) in the ferrite matrix at 250ºC for 1 s. However, DSA presents itself as multiple serrations and repeated events in the stress-strain curves. For this repeated action, dislocations should slow down due to some obstacles and re-pinned by the solute atoms. The temperature change also influences the kinetics of the dislocations, however it is very low compared to the effect of the temperature on the solutes (Carbon in a DP steel). Thus, the influence of temperature on dislocations are neglected in our assumption. To understand the details of this phenomenon, we need a model for the dislocation motion. Assuming that slip mainly occurs in ferrite phase with b = 0.255 nm, the dislocation velocity can be calculated by the Orowan's equation which is still valid for the phase mixture while considering the steel as an ideal composite under iso-strain conditions :

$$\dot{\gamma} = \rho b V \tag{5}$$

where the shear strain rate is linked to the tensile strain rate by the Taylor factor, $\dot{\gamma} = M\dot{\varepsilon}$. In the Orowan's equation, the dislocation velocity, *V*, strongly depends on the density, which should be measured with certain precision for accurate velocity calculations. For a DP steel, several different dislocation velocities such as the velocity in ferrite and martensite can be defined. In this study, *V* is considered as the time-average velocity of the dislocations of the overall phase mixture based on the compliance with the experimental findings.

According to the modified Warren-Averbach measurements in DP590, dislocation density in the as-received condition starts at 3 x 10^{14} m^{-2}, and increases to 4 x 10^{14} m^{-2} with ~ 10% strain. These measured densities, however, are an average of martensitic and ferritic regions, as it is not possible to do a separate x-ray analysis for each phase.

In previous works on DP steels, the geometrically necessary dislocations (GND) density in ferrite has been measured to be 2.5 x 10^{13} m^{-2} [47]. In addition to GND in the grain interior, the interface of the ferrite and martensite contains a high amount of GND with a density of 2.5 x 10^{14} m^{-2} [47].

These dislocations are emitted to accommodate the volume change due to the austenite to martensite phase transformation during the heat treatment. They are also necessary for the compatibility of the ferrite and martensite phases during the deformation [84]. TEM measurements, on the other hand, include statistically stored dislocations (SSD) in addition to GND and yield values close to 10^{15} m^{-2} [56]. The modified Warren-Averbach technique used in this study correlates well with the GND density at the interface. With its higher martensite fraction and ferrite-martensite interface area, DP800 has a higher dislocation density of 6 x 10^{14} m^{-2}, confirming the sensitivity of the measurements to the GND. Indeed, the strain hardening and flow behavior of DP steels can truly be modeled with the consideration of the GND [46,85]. Our measurements provided no information on the type (GND or SSD) or the nature (mobile or sessile) of the dislocation, yet the density values seem to include both types. Independent of their nature, they should resist the motion of mobile dislocations and should be accounted in Orowan's equation. Therefore, our assumption is to incorporate the dislocation density as measured.

Martensite is assumed to be non-contributing in the plastic deformation due to its stiff nature, where our suggested model is defined in ferrite. However, martensite could become a resisting obstacle against moving dislocations at the interphases. More amount of martensite encircled around ferrite could increase the materials brittleness and lead towards fracture under deformation. However, this influence of martensite is not related with DSA and leads directly to fracture. Therefore it should not be confused comparing to DSA.

When the dislocation density and velocities are available, the distance traveled by the dislocations between the obstacles can be calculated from the serrations in the stress-strain curves. Figure 31 zooms into the serrations in both steels at various testing conditions.

For each condition, strain between two consecutive serrations gives the time for dislocation travel before pinning, $t = \Delta\varepsilon/\dot{\varepsilon}$. Combined with the velocity, the time gives the characteristic distance, $d = Vt$. While it is hard to capture the consecutive serrations in DP800, they are clear in DP590. For DP590, the strain, and therefore time, between consecutive serrations consistently increases as the test progresses (Figure 31). This may indicate a change in the characteristic length at a constant velocity. However, dislocations slow down as their density increases with the strain. The distances should be adjusted according to the new velocities.

For DP590 deforming at 200ºC and 0.01 s^{-1}, the dislocation velocity is 4 x 10^{-7} m/s at the beginning of the test and decreases to 2.8 x 10^{-7} m/s at 10% strain. The characteristic length for the first interval ($\Delta\varepsilon$ = 0.0076 and t = 0.76 s) becomes 0.30 μm. After adjusting for the velocity change, the distance for the second interval ($\Delta\varepsilon$ = 0.0202 and t = 2.02 s) becomes 0.56 μm. Considering the error in the dislocation density measurements and the velocity calculations, this change in the length is within the acceptable limits. For DP590 deforming at 300ºC and 0.1 s^{-1}, the characteristic length for the third interval ($\Delta\varepsilon$ = 0.0045 and t = 0.045 s) is 0.18 μm and 0.20 μm for the fourth interval ($\Delta\varepsilon$ = 0.0074 and t = 0.074 s). In this case, change in the distance is negligible, suggesting almost a fixed spacing for the obstacles. Serrations at 300ºC and 1 s^{-1} (fifth = 0.36 μm, sixth = 0.30 μm, and seventh = 0.50 μm) again indicate a fixed and consistent characteristic length almost independent from strain rate, strain and temperature.

The consistent measurements of the characteristic length suggest that it is associated to a sub-micron scale, quasi-periodic microstructural feature. Such possible features can be precipitates common in these steels [86–88], inclusions [87], grain boundaries, cell walls [45], and shear bands [56].

While an advanced characterization study is needed to pinpoint the actual source of serrations, our most likely candidates are the cell walls and the shear bands. Deformation in DP steels mostly concentrates to the ferrite phase [44] and generates a high concentration of stored and geometrically necessary dislocations [84]. These dislocations rearrange themselves into cells and other substructures early in the deformation, just after 2% strain. The cell size decreases as the deformation progresses and the cell walls become sharper and manifest themselves as the strain bands in the ferrite [45]. The typical cell size after 2% strain corresponds to 1 μm and correlates with the characteristic distance in our calculations. Therefore, we suggest the cell walls as potential obstacles for the dislocation motion. Formation of shear bands in the ferrite grains has recently been shown with mesoscale finite element simulations incorporating the GND activity during the deformation [46]. The distance between the shear bands also align with the size of dislocation substructures [46] (Figure 13, Chapter 2) and our measurements.

The higher dislocation density and the slower deformation rate result in a dislocation velocity of 2×10^{-8} m/s in DP800 tested at 300ºC and 0.001 s^{-1}. This velocity yields a characteristic distance of 0.17 μm for the eight interval ($\Delta\varepsilon$ = 0.0086 and t = 8.6 s) in Figure 13. The distance in DP800 at 300ºC matches well with the distance in DP590 at 300ºC. This remarkable match of the distance in separate steels having similar ferrite sizes (9.3 vs. 8.7 μm) supports our theory of periodic microstructural features are responsible for the DSA behavior and the serrations. Additionally, this similarity of the ferrite grain sizes eliminates the possible influence of the grain size difference on comparison of the two grades. While the main aim of this paper is to present extensive experimental results together with a very simple model for the occurrence of DSA at industrially relevant conditions, suggested approach is enough for a rough estimation of the frequency of serrations.

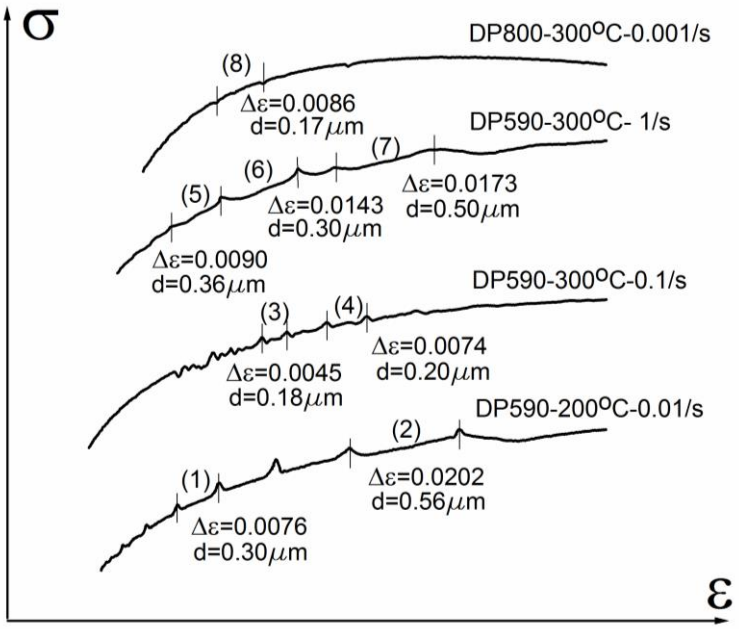

Figure 31 Details of the serrations in DP590 and DP800. Note that the curves are not drawn in scale to each other.

CHAPTER 5

SUMMARY & FUTURE WORKS

Mechanical testing of DP590 and DP800 steels between RT - 400ºC and 0.001 – 1 s^{-1} revealed two types of deformation behavior for given temperature ranges. While RT, 100ºC and 400ºC behavior were ordinary, 200ºC - 300ºC was controlled by the DSA and had severe consequences for the formability. A detailed analysis of the stress-strain curves and the x-ray measurements identified the microstructural mechanisms responsible from the DSA. Key findings of this study are summarized below:

1) Both grades of the steels can be formed up to 100ºC and 1 s^{-1}. There is slight softening in the strength at this temperature with minimal loss in the uniform and total ductility. Softening is significant at 400ºC, but uniform strain decreases considerably. Both the uniform and total ductility are independent of the strain rate at RT, 100ºC and 400ºC.

2) There is no softening in the strength in the DSA controlled deformation between the cold forming temperatures 200ºC - 300ºC. The common symptom of DSA is the serrations in the stress-strain curves. They are more evident in DP590 due its higher ferrite content, but both materials suffer from the DSA at the same extent. Increasing strain rates and temperatures intensify the effects of DSA on the ductility and result in almost 35% decrease in uniform and total ductility of both grades. Although DP800 does not show visual curves consisting serrations, both grades have negative strain rate sensitivities within the DSA range (m = -0.017 for DP590 and -0.006 for DP800), which recovers to positive values with the increasing temperature.

Combined with low uniform strains, the negative *m* values should result in a poor formability. Therefore, warm forming (or deformation heating at high strain rates) should be avoided in both grades.

3) Serrations in the stress-strain curves give the time between consecutive pinning of the dislocations by the solute atoms. When combined with the dislocation velocities calculated from the dislocation densities, this time yields a similar characteristic length in both grades. The consistent measurements of the length ($d \approx 0.3$ μm) suggest that the serrations are associated to a sub-micron scale, quasi-periodic microstructural feature. Moreover, the consistent measurements of the length ($d \approx 0.3$ μm) in two grades show that the volume fraction of the phases do not influence the DSA mechanism. Therefore, the DSA mechanism is estimated to be more dependent on the ferrite grain size rather than the ferrite volume fraction. The most likely candidates for such features are the dislocations cells and substructures commonly observed in DP steels.

4) Our future work is to develop a mesoscale model coupled with characterization experiments, which will provide better explanations for the behavior along with better accuracy in predictions.

REFERENCES

[1] 2017 Jeep Renegade Body Structure - Boron Extrication, http://www.boronextrication.com/2017/03/26/2017-jeep-renegade-body-structure/ (accessed July 21, 2017).

[2] Advanced Materials in Automotive - Advanced Manufacturing, http://advancedmanufacturing.org/advanced-materials-automotive/ (accessed July 21, 2017).

[3] 2016 Honda Civic Body Structure - Boron Extrication, http://www.boronextrication.com/2015/12/23/2016-honda-civic-body-structure/ (accessed July 21, 2017).

[4] 2017 Lincoln Continental Body Structure - Boron Extrication, http://www.boronextrication.com/2017/01/09/2017-lincoln-continental-body-structure/ (accessed July 21, 2017).

[5] A. Abraham, Metallic Material Trends in the North American Light Vehicle Ducker Worldwide Introduction, (2015).

[6] R. Kuziak, R. Kawalla, S. Waengler, Advanced high strength steels for automotive industry, Arch. Civ. Mech. Eng. 8 (2008) 103–117.

[7] T.B. Hilditch, T. de Souza, P.D. Hodgson, Properties and automotive applications of advanced high-strength steels (AHSS), Elsevier Ltd, 2015.

[8] Overview of Major Steels, https://www.tf.uni-kiel.de/matwis/amat/iss/kap_9/advanced/t9_2_1b.html (accessed July 21, 2017).

[9] Laws & Regulations | NHTSA, https://www.nhtsa.gov/laws-regulations (accessed August 28, 2017).

[10] C.M. Tamarelli, AHSS 101: the evolving use of advanced high-strength steel for automotive applications, Steel Mark. Dev. Inst. (2011) 42.

[11] C.C. Tasan, M. Diehl, D. Yan, M. Bechtold, F. Roters, L. Schemmann, C. Zheng, N. Peranio, D. Ponge, M. Koyama, K. Tsuzaki, D. Raabe, An Overview of Dual-Phase Steels: Advances in Microstructure-Oriented Processing and Micromechanically Guided Design, Annu. Rev. Mater. Res. 45 (2014) 391-431.

[12] X.L. Cai, A.J. Garratt-Reed, W.S. Owen, The development of some dual-phase steel structures from different starting microstructures, Metall. Trans. A. 16 (1985) 543–557.

[13] S. Kim, S. Lee, Effects of martensite morphology and volume fraction on quasi-static and dynamic deformation behavior of dual-phase steels, Metall. Mater. Trans. A. 31 (2000) 1753–1760.

[14] K. Nakajima, T. Urabe, Y. Hosoya, S. Kamiishi, T. Miyata, N. Takeda, Influence of Microstructural Morphology and Prestraining on Short Fatigue Crack Propagation in Dual-phase Steels, ISIJ Int. 41 (2001) 298–305.

[15] G.R. Speich, V. a. Demarest, R.L. Miller, Formation of Austenite During Intercritical Annealing of Dual-Phase Steels, Metall. Trans. A. 12 (1981) 1419–1428.

[16] S. Sun, M. Pugh, Properties of thermomechanically processed dual-phased steels containing fibrous martensite, Mater. Sci. Eng. A. 335 (2002) 298–308.

[17] Y. Cao, B. Karlsson, J. Ahlström, Temperature and strain rate effects on the mechanical behavior of dual phase steel, Mater. Sci. Eng. A. 636 (2015) 124–132.

[18] S. Curtze, V.T. Kuokkala, M. Hokka, P. Peura, Deformation behavior of TRIP and DP steels in tension at different temperatures over a wide range of strain rates, Mater. Sci. Eng. A. 507 (2009) 124–131.

[19] R.R.U. Queiroz, F.G.G. Cunha, B.M. Gonzalez, Study of dynamic strain aging in dual phase steel, Mater. Sci. Eng. A. 543 (2012) 84–87.

[20] A. Das, M. Ghosh, S. Tarafder, S. Sivaprasad, D. Chakrabarti, Micromechanisms of deformation in dual phase steels at high strain rates, Mater. Sci. Eng. A. 680 (2017) 249–258.

[21] N.D. Beynon, S. Oliver, T.B. Jones, G. Fourlaris, Tensile and work hardening properties of low carbon dual phase strip steels at high strain rates, Mater. Sci. Technol. 21 (2005) 771–778.

[22] H. Huh, S.B. Kim, J.H. Song, J.H. Lim, Dynamic tensile characteristics of TRIP-type and DP-type steel sheets for an auto-body, Int. J. Mech. Sci. 50 (2008) 918–931.

[23] Larour P (2010), Strain Rate Sensitivity of Automotive Sheet Steels (Doctoral Dissertation).
Retrieved from http://publications.rwth-aachen.de/record/94600/files/3271.pdf

[24] Y. Gao, C. Xu, Z. ping He, Y. lin He, L. Li, Response characteristics and adiabatic heating during high strain rate for TRIP steel and DP steel, J. Iron Steel Res. Int. 22 (2015) 48–54.

[25] A. Ekrami, High temperature mechanical properties of dual phase steels, Mater. Lett. 59 (2005) 2070–2074.

[26] A.K. Sachdev, Dynamic Strain Aging of Various Steels, Metall. Trans. A. 13 (1982) 1793–1797.

[27] D.J. Llewellyn, D. T., Hillis, Dual Phase Steels, Ironmak. Steelmak. 23 (1996) 471–478.

[28] R. Rana (2016), Automotive Steels: Design, Processing and Applications, Woodhead Publishing.

[29] O.N. Mohanty, (2017). Forging Grade Steels for Automotives.
In: R. Rana & S. B. Singh (Eds.) Automotive Steels: Design, Metallurgy, Processing and Applications, Woodhead Publishing, (pp. 413 - 448).

[30] H.C. Chen, G.H. Cheng, Effect of martensite strength on the tensile strength of dual phase steels, J. Mater. Sci. 24 (1989) 1991–1994.

[31] T.G. Koo, J Y, Young M.J., On the law of mixtures in dual-phase steels, Metall. Trans. A. 11A (1980) 852–854.

[32] R.G. Davies, Influence of martensite composition and content on the properties of dual phase steels, Metall. Trans. A. 9 (1978) 671–679.

[33] M.J. Molaei, A. Ekrami, The effect of dynamic strain aging on fatigue properties of dual phase steels with different martensite morphology, Mater. Sci. Eng. A. 527 (2009) 235–238.

[34] R.L. Speich, G. R., Miller, Structure and properties of dual-phase steels, TMS-AIME, in: 1979: pp. 145–182.

[35] M.S. Rashid, Dual phase steels, Ann. Rev. Mater. Sci. 11 (1981) 245–266.

[36] O.A. Girina, N.M. Fonstein, Influence of Al Additions on Austenite Decomposition in Continuously Annealed Dual-Phase Steels, Mater. Sci. Technol. (2005) 65–76.

[37] L.A. Fréchard S., Redjaïmia A. , Lach E., Mechanical behaviour of nitrogen-alloyed austenitic stainless steel hardened by warm rolling, Mater. Sci. Eng. A. 415 (2006) 219–224.

[38] T. Senuma, Physical Metallurgy of Modern High Strength Steel Sheets, ISIJ Int. 41 (2001) 520–532.

[39] J.D. Embury, J.L. Duncan, Formability of Dual-Phase Steels, JOM J. Miner. Met. Mater. Soc. 34 (1982) 24–29.

[40] J.H. Butler, J. F., Bucher, Vanitec Seminar on Vanadium Cold Pressing and Dual-Phase Steels, 1978, W. Berlin, Germany.

[41] Uenishi, Y. Kuriyama, M. Usuda, M. Suehiro, Improvement of Crashwothiness by Application of High Strength Steel for Light weight Auto Bodies, proc. Int. Body Eng. Conf. (IBEC'96) on Automotive Body Interior & Safety Systems Vol.23, Automotive Technology Group, Michigan, 1996.

[42] The unique characteristics of dual-phase steels, D.J. Schaeffler. http://www.thefabricator.com/article/metalsmaterials/the-unique-characteristics-of-dual-phase-steels/ (accessed July 27,2017).

[43] S.K. Paul, Theoretical analysis of strain- and stress-based forming limit diagrams, J. Strain Anal. Eng. Des. 48 (2013) 177–188.

[44] W.S. Sarosiek, A. M., Owen, The work hardening of dual-phase steels at small plastic strains, Mater. Sci. Eng. 66 (1984) 13–34.

[45] D.A. Korzekwa, D.K. Matlock, G. Krauss, Dislocation substructure as a function of strain in a dual-phase steel, Metall. Trans. A. 15 (1984) 1221–1228.

[46] A. Ramazani, K. Mukherjee, A. Schwedt, P. Goravanchi, U. Prahl, W. Bleck, Quantification of the effect of transformation-induced geometrically necessary dislocations on the flow-curve modelling of dual-phase steels, Int. J. Plast. 43 (2013) 128–152.

[47] J. Kadkhodapour, S. Schmauder, D. Raabe, S. Ziaei-Rad, U. Weber, M. Calcagnotto, Experimental and numerical study on geometrically necessary dislocations and non-homogeneous mechanical properties of the ferrite phase in dual phase steels, Acta Mater. 59 (2011) 4387–4394.

[48] M. Calcagnotto, D. Ponge, E. Demir, D. Raabe, Orientation gradients and geometrically necessary dislocations in ultrafine grained dual-phase steels studied by 2D and 3D EBSD, Mater. Sci. Eng. A. 527 (2010) 2738–2746.

[49] G.R. Speich, Fundamentals of dual-phase steels, in: TMS-AIME, Warrendale, PA, 1981: pp. 3–45.

[50] Y. Gao, H., Huang, Geometrically necessary dislocation and size-dependent, Scr. Mater. 48 (2003) 113–118.

[51] U.F. Kocks, A statistical theory of flow stress and work-hardening, Philos. Mag. 13 (1966) 541–566.

[52] M. Zaiser, E.C. Aifantis, Geometrically necessary dislocations and strain gradient plasticity—a dislocation dynamics point of view, Scr. Mater. 48 (2003) 133–139..

[53] E. Van der Giessen, A. Needleman, GNDs in nonlocal plasticity theories: lessons from discrete dislocation simulations, Scr. Mater. 48 (2003) 127–132.

[54] A. Needleman, J.G. Sevillano, Preface to the viewpoint set on: geometrically necessary dislocations and size dependent plasticity, Scr. Mater. 48 (2003) 109–111.

[55] H. Larson, B. C., Yang, W., Tischler J. Z., Ice G. E., Budai J. D., Lui W., Weiland, Micron-resolution 3-D measurement of local orientations near a grain boundary in a plane-strained aluminum using X-ray microbeams, Int. J. Plast. 20 (2004) 543–560.

[56] W.S. Cai, X. L., Feng J.., Owen, The dependence of some tensile and fatigue properties of a dual-phase steel on its microstructure, Metall. Trans. A. 16 (1985) 1405–1415.

[57] C.J. Gardner, B.L. Adams, J. Basinger, D.T. Fullwood, EBSD-based continuum dislocation microscopy, Int. J. Plast. 26 (2010) 1234–1247.

[58] T. Ungár, S. Ott, P.. Sanders, A. Borbély, J.. Weertman, Dislocations, grain size and planar faults in nanostructured copper determined by high resolution X-ray diffraction and a new procedure of peak profile analysis, Acta Mater. 46 (1998) 3693–3699.

[59] W.M. Lomer, The yield phenomenon in polycrystalline mild steel, J. Mech. Phys. Solids. 1 (1952) 64–73.

[60] A.H. Cottrell, B.A. Bilby, Dislocation Theory of Yielding and Strain Ageing of Iron, Proc. Phys. Soc. Sect. A. 62 (1949) 49.

[61] J. Baird, The effects of strain-aging due to interstitial solutes on the mechanical properties of metals, Review 149, Metall. Rev.5 (1971) 1-18.

[62] A.S. Key, Y. Nakada, W.C. Leslie, Dynamic strain ageing in iron and steel, in: A.R. Rosenfield, G.T. Hahn, A.L. Bement Jr., R.I. Jaffee (Eds.), Dislocation Dynamics, Mc Graw-Hill Book Company, New York, 1968, pp. 381-408.

[63] G.T. (Rusty) Gray, High-Strain-Rate Deformation: Mechanical Behavior and Deformation Substructures Induced, Annu. Rev. Mater. Res. 42 (2012) 285–303.

[64] R.W. Armstrong, S.M. Walley, High strain rate properties of metals and alloys, International Materials Reviews. 53 (2008) 105 - 128.

[65] F. Ozturk, S. Toros, S. Kilic, Tensile and Spring-Back Behavior of DP600 Advanced High Strength Steel at Warm Temperatures, J. Iron Steel Res. Int. 16 (2009) 41–46.

[66] A. Portevin, M. Le Chatelier, Tensile tests of alloys undergoing transformation, Comptes Rendus Acad. Sci. 176 (1923) 507-510.

[67] A.K. Taheri, T.M. Maccagno, J.J. Jonas, Effect of cooling rate after hot rolling and of multistage strain aging on the drawability of low-carbon-steel wire rod, Metall. Mater. Trans. A. 26 (1995) 1183–1193.

[68] P. Verma, G. Sudhakar Rao, P. Chellapandi, G.S. Mahobia, K. Chattopadhyay, N.C. Santhi Srinivas, V. Singh, Dynamic strain ageing, deformation, and fracture behavior of modified 9Cr-1Mo steel, Mater. Sci. Eng. A. 621 (2015) 39–51.

[69] S.-J. Lee, J. Kim, S.N. Kane, B.C. De Cooman, On the origin of dynamic strain aging in twinning-induced plasticity steels, Acta Mater. 59 (2011) 6809–6819.

[70] C.C. Li, W.C. Leslie, Effects of dynamic strain aging on the subsequent mechanical properties of carbon steels, Metall. Trans. A. 9 (1978) 1765–1775.

[71] J. Robinson, M. Shaw, Microstructural and mechanical influences on dynamic strain aging phenomena, Int. Mater. Rev. 39 (1994) 113-122.

[72] M.S. Shahriary, B. Koohbor, K. Ahadi, A. Ekrami, M. Khakian-Qomi, T. Izadyar, The effect of dynamic strain aging on room temperature mechanical properties of high martensite dual phase (HMDP) steel, Mater. Sci. Eng. A. 550 (2012) 325–332.

[73] P. Rodriguez, Serrated plastic flow, Bull. Mater. Sci. 6 (1984) 653–663.

[74] A. Bintu, G. Vincze, C.R. Picu, A.B. Lopes, J.J. Grácio, F. Barlat, Strain hardening rate sensitivity and strain rate sensitivity in TWIP steels, Mater. Sci. Eng. A. 629 (2015) 54–59.

[75] H.K. Yang, Y.Z. Tian, Z.J. Zhang, Z.F. Zhang, Different strain rate sensitivities between Fe–22Mn–0.6C and Fe–30Mn–3Si–3Al twinning-induced plasticity steels, Mater. Sci. Eng. A. 655 (2016) 251–255.

[76] K. J.-K., L. Chen, H. Kim, S. Kim, G.S. Kim, Y. Estrin, B.C. De Cooman, Strain Rate Sensitivity of C-alloyed, High-Mn, Twinning-induced Plasticity Steel, Doi.org. 80 (2009) 493–498.

[77] S. L. Mannan, K. G. Samuel, P. Rodriguez, Dynamic strain ageing in type 316 stainless steel, Trans. Indian Inst. Metals, 36 (1983) 313-320.

[78] Program for Qualitative and Quantitative Powder X-Ray Diffraction Analysis. http://www.xpowder.com/download/xpowder.pdf (accessed March 25, 2017).

[79] T. Ungár, I. Dragomir, Á.;. Révész, A. Borbély, The contrast factors of dislocations in cubic crystals: the dislocation model of strain anisotropy in practice, J. Appl. Crystallogr. 32 (1999) 992–1002.

[80] T. Shintani, Y. Murata, Evaluation of the dislocation density and dislocation character in cold rolled Type 304 steel determined by profile analysis of X-ray diffraction, Acta Mater. 59 (2011) 4314–4322.

[81] N. Tsuchida, Y. Izaki, T. Tanaka, K. Fukaura, Effects of Temperature and Strain Rate on Stress-Strain Curves for Dual-Phase Steels and Their Calculations by Using the Kocks-Mecking Model, ISIJ Int. 52 (2012) 729–734.

[82] A.S. Khan, M. Baig, S.-H. Choi, H.-S. Yang, X. Sun, Quasi-static and dynamic responses of advanced high strength steels: Experiments and modeling, Int. J. Plast. 30 (2012) 1–17.

[83] R. bo Song, Q. feng Dai, Dynamic deformation behavior of dual phase ferritic-martensitic steel at strain rates from 10-4 to 2000 s-1, J. Iron Steel Res. Int. 20 (2013) 48–53.

[84] M.F. Ashby, The deformation of plastically non-homogeneous materials, Philos. Mag. 21 (1970) 399–424.

[85] U. Liedl, S. Traint, E.A. Werner, An unexpected feature of the stress-strain diagram of dual-phase steel, Comput. Mater. Sci. 25 (2002) 122–128.

[86] S.P. Tsai, C.H. Jen, H.W. Yen, C.Y. Chen, M.C. Tsai, C.Y. Huang, Y.T. Wang, J.R. Yang, Effects of interphase TiC precipitates on tensile properties and dislocation structures in a dual phase steel, Mater. Charact. 123 (2017) 153–158.

[87] H. Askari, H.M. Zbib, X. Sun, Multiscale modeling of inclusions and precipitation hardening in metal matrix composites: Application to advanced high-strength steels, ASCE J. Nanomech. Micromech. 3 (2013) 24–33.

[88] L.C. Zhang, I.B. Timokhina, A. La Fontaine, S.P. Ringer, P.D. Hodgson, E. V. Pereloma, Effect of pre-straining and bake hardening on the microstructure and mechanical properties of CMnSi TRIP steels, Metall. Ital. 101 (2009) 49–55.